Scanning tunnelling microscopy investigations of simple surface reactions on Rh(110)

2006 J. Phys.: Condens. Matter 18 R387

(http://iopscience.iop.org/0953-8984/18/22/R01)

INSTITUTE OF PHYSICS PUBLISHING JOURNAL OF PHYSICS: CONDENSED MATTER

J. Phys.: Condens. Matter **18** (2006) R387–R416 doi:10.1088/0953-8984/18/22/R01

TOPICAL REVIEW

Scanning tunnelling microscopy investigations of simple surface reactions on Rh(110)

Cristina Africh and Giovanni Comelli

Department of Physics and Center of Excellence for Nanostructured Materials, University of Trieste, I-34127 Trieste, Italy
and
Laboratorio TASC INFM-CNR, Area Science Park, I-34012 Basovizza-Trieste, Italy

Received 16 February 2006, in final form 31 March 2006
Published 16 May 2006
Online at stacks.iop.org/JPhysCM/18/R387

Abstract

The unique potential of scanning tunnelling microscopy (STM) as a tool for determining the elementary steps of surface catalytic reactions at an atomic scale is highlighted using selected representative results obtained in studies of adsorption and reactions on the Rh(110) surface. The Rh(110) surface was chosen as a prototype of a flexible catalyst, due to its propensity to reconstruct in the presence of adsorbates. Both dissociative adsorption of simple molecules and oxidation reactions involving adsorbed oxygen layers are considered. It was demonstrated that a combined approach where STM was used in conjunction with other experimental techniques and *ab initio* calculations yields a thorough description of the underlying reaction mechanism.

Contents

1. Introduction 388
2. Adsorbate induced Rh(110) structures 389
   2.1. Interaction of oxygen with the Rh(110) surface 389
   2.2. Interaction of nitrogen with the Rh(110) surface 391
   2.3. Comparison with other transition metal fcc (110) surfaces 392
3. Surface reactions on Rh(110) 392
   3.1. Dissociative adsorption on Rh(110) 393
   3.2. Reactions of adsorbed oxygen layers on Rh(110) 397
4. Conclusions 410
5. Outlook 411
Acknowledgments 412
References 412

0953-8984/06/220387+30$30.00

1. Introduction

Advances in heterogeneous catalysis have become a key issue for providing both new energy sources and environment protection. In this respect, fundamental research at surfaces and interfaces should provide in-depth knowledge of all catalytically relevant processes, capturing events at the atomic scale. Successful exploitation of this knowledge enables further development and improvement of catalysts' performance.

Catalytic processes can generally be subdivided into a sequence of interrelated events: adsorption of the reactants, surface and subsurface diffusion, interaction between adsorbed species, and desorption of products. Since real catalysts are complex systems, mainly powders, often composed of metal particles supported or encapsulated by an oxide matrix or suspended in colloidal solutions, simplified model systems, such as metal single crystals or thin films, are used to study the single events involved in the surface reactions. This fundamental 'bottom-up' approach to catalysis has been one of the major subjects of surface science, enabled by the continuous development of a great variety of surface sensitive methods.

In this context scanning tunnelling microscopy (STM) has proven since its early days to be an extremely powerful technique. In the years 1992–1994, the pioneering papers on STM studies of catalytic reactions on metal surfaces, addressing the mechanisms of simple surface reactions at the atomic scales, appeared in the literature [1–3]. A wealth of similar studies followed [4–7], moving towards more complex reactions, involving organic molecules [8–11]. With continuous improvement of the quality of STM imaging, the STM has been used with success for studies of more complicated oxide surfaces (see for example [12]), supported metal clusters [13, 14], and so-called 'inverse model catalysts' [15].

One of the advantages of STM is its capability of imaging features at different length scales, from a few microns down to a few nanometres, which makes it possible to investigate different dimensional aspects of the same phenomenon. This possibility has been exploited, for instance, in the case of the water formation reaction on a Pt(111) surface [16]. In this study, the propagation of the reaction fronts was followed on large length-scales, while small-area images provided information about the reaction mechanism inside the reaction front at an atomic scale. Thus the two approaches (large scale/small scale) allowed the authors to give a complete picture of the process. This study is also an excellent illustration of the potential of STM for direct imaging of the dynamics of surface reactions during their evolution.

Another distinct characteristic of STM, which makes it a unique tool, is that it can provide atomic-scale structural information on a surface in different environments, i.e. in vacuum, atmospheric pressure and liquids. In fact, the recent high-pressure STM studies demonstrated that the relation between surface structure and catalytic activity can be fully explored [17–22]. Another very important field is electrocatalysis, where STM yields information both on the structural determination of electrode surfaces and of adlayers in solution [23] and on reactions in solution (see for example [24]). The application of the technique, complemented by other tools, contributed to gain new insight into performance of realistic catalytic systems, such as fuel cells [25, 26], electropromoted reactors [27], and corrosion processes [28].

In brief, STM is a very powerful technique for studying surface reactions at the atomic level and its applications are expanding beyond catalysis and corrosion phenomena, because it is recognized that the structural modifications induced by surface reactions affect dramatically the surface properties.

Besides all these positive features, however, we should note that STM images do not provide information on the chemical identity of the ad-species, which requires complementary techniques and theoretical simulations for unequivocal interpretation of the data.

Rhodium is widely used in catalytic applications. Heterogeneous Rh containing catalysts are mounted in car converters, where Rh is the key element for promoting NO dissociation [29]. This application is certainly the most relevant since it accounts for more than 85% of the global worldwide rhodium demand [30].

Among the low indexed Rh single crystal surfaces, the (110) surface is a perfect example of a flexible surface [31], which easily reconstructs upon chemisorption. On Rh(110), hence, it is possible to study how a surface restructures, changing its reactivity, as a reaction proceeds. In this report, we concentrate in particular on oxygen and nitrogen involving reactions. Since these reactions have already been studied with a wide range of experimental techniques [32, 33], STM data can be interpreted in detail, yielding a great amount of information. The interest in the interaction with oxygen and nitrogen can be traced back first of all to the important role of rhodium in the selective conversion of NO to N_2. On a more fundamental side, both adsorbates form strong bonds with rhodium atoms, inducing competitive reconstructions, and it has been possible to investigate the influence of such competitiveness on reactivity. Furthermore, oxygen gives the possibility to follow the whole transition from low adsorbate coverage on a metal substrate to surface oxides, which play a decisive role in the reactivity of a surface, as shown, for example, for ruthenium [34–37]. In this contest, UHV studies of simple surface reactions are still essential to gain precise knowledge of the detailed mechanism of the overall processes.

The review is organized as follows. Section 2 summarizes the existing knowledge about the interaction of the rhodium surface with oxygen and nitrogen, which was the basis for the investigations of the surface reactions described in section 3. Section 3 is the essential part of the review describing results obtained by our group and other laboratories concerning dissociative adsorption (section 3.1) and reactions of oxygen adlayers (section 3.2). Conclusive remarks, highlighting the role of STM in elucidating reaction mechanisms, and an outlook on future developments to expand the exploration range of STM in studies of surface reactions are the topics of sections 4 and 5, respectively.

2. Adsorbate induced Rh(110) structures

In the following, we describe firstly the structures generated by oxygen adsorption on the Rh(110) surface and then those produced by nitrogen. It will be shown that both adsorbates induce missing row reconstructions of the surface but the details of the interaction are markedly different. While oxygen preserves the close-packed metal rows, without being incorporated within the metal layer but simply decorating the rows, nitrogen is incorporated between the metal atoms, preventing the formation of close-packed metal rows. As a consequence, reconstruction occurs in different directions: $(1 \times n)$ type for O and $(n \times 1)$ for N. Differences and analogies with other transition metal fcc (110) surfaces are finally reported.

2.1. Interaction of oxygen with the Rh(110) surface

On Rh(110), dissociative adsorption of molecular oxygen occurs at temperatures above 100 K, with atomic oxygen forming a variety of ordered structures [32]. O_2 adsorption at 100 K $<$ T $<$ 300 K does not involve any substrate reconstruction. When the coverage approaches 1 ML, an ordered $(2 \times 1)\,p2mg$-O structure is observed. Figure 1(a) shows an STM image and a schematic model of the structure. In this structure O atoms sit in threefold sites along the $[1\bar{1}0]$ rows in a *zigzag* fashion and are therefore coordinated by two surface atoms and a second layer Rh atom [38–40].

If the temperature is high enough to allow the diffusion of Rh atoms on the surface (∼400 K), O induced structures involve a reconstruction of the substrate [41]. In particular, as the O coverage increases, the surface undergoes $(1 \times n)$ reconstructions (n = 2–5), where

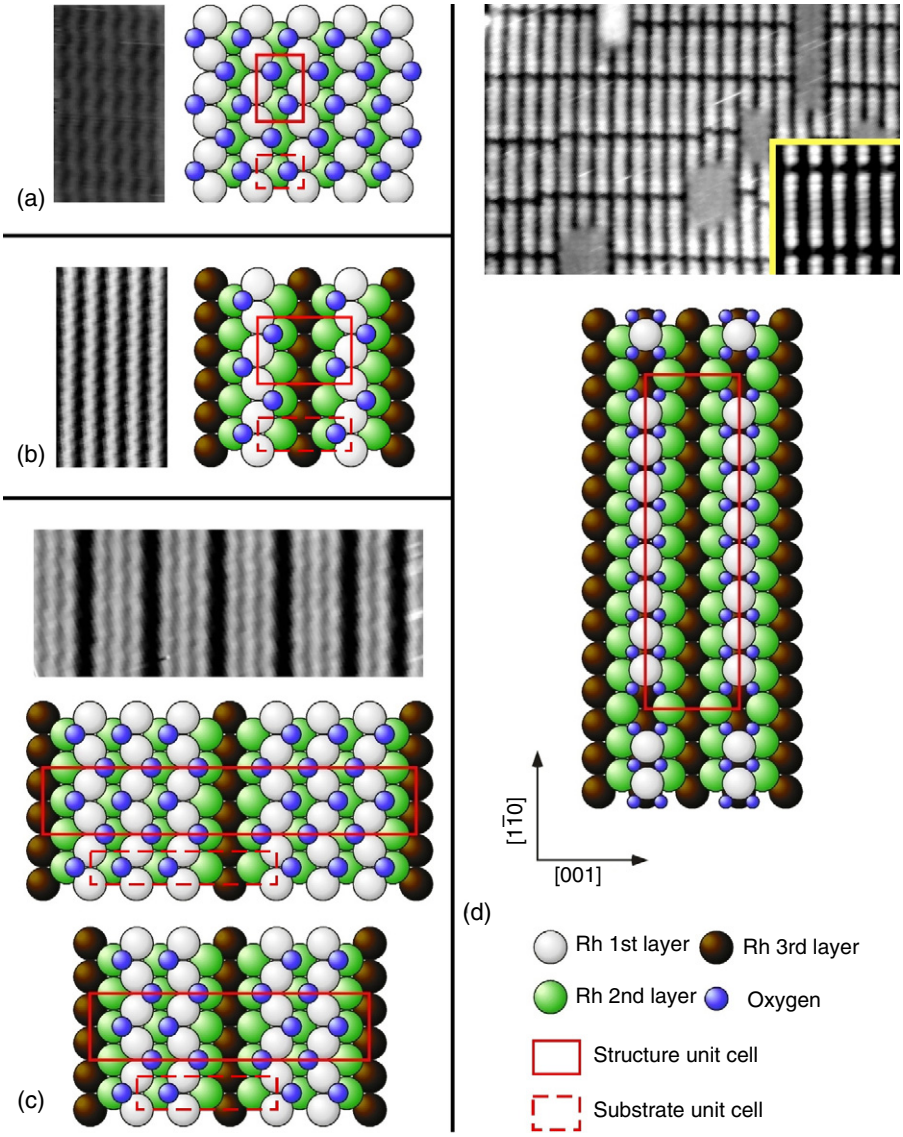

Figure 1. STM images and corresponding models of oxygen structures on Rh(110): (a) (2 × 1) $p2mg$-O on unreconstructed substrate; (b) (2 × 2) $p2mg$-O on (1 × 2) substrate; (c) c(2 × 8)-O on (1 × 4) and c(2 × 6)-O on (1 × 3) (right side of the STM image); (d) (10 × 2)-O (inset: zoom of the segments). (Image parameters: (a) 2.3 × 4.1 nm^2, $V_B = +0.16$ V, $I = 0.46$ nA; (b) 3.8 × 7.0 nm^2, $V_B = +0.36$ V, $I = 0.95$ nA; (c) 8.9 × 3.3 nm^2, $V_B = +0.54$ V, $I = 1$ nA; (d) 17.5 × 11.4 nm^2, $V_B = +0.60$ V, $I = 0.71$ nA. Inset: 4.2 × 4.4 nm^2, $V_B = +0.63$ V, $I = 1.02$ nA.)

one close-packed [1$\bar{1}$0] row out of n is missing and all the remaining rows are decorated by O in threefold sites in a *zigzag* fashion. O coverage of 0.5 ML, 0.67 ML, 0.75 ML, and 0.8 ML leads to (1 × 2), (1 × 3), (1 × 4), and (1 × 5) reconstructions of the substrate, resulting in (2 × 2) $p2mg$, c(2 × 6), c(2 × 8), and c(2 × 10) oxygen structures respectively.

Selected representative oxygen-induced structures on Rh(110) and the corresponding STM images are shown in figure 1. Figure 1(b) shows an STM image and the model of the

$(2 \times 2)p2mg$-O structure. The metal close-packed rows are imaged as bright rows, while oxygen atoms are imaged as depressions (which is the usual contrast for this adsorbate on metal surfaces) and are responsible for the *zigzag* appearance of the rows. As the image clearly shows, the *zigzag* phase is generally preserved between adjacent rows [42, 43].

Figure 1(c) illustrates the c$(2 \times 2n)$-O structures, which are obtained by dosing more oxygen on the $(2 \times 2)p2mg$-O at $T \geqslant 650$ K. In these structures, *zigzag* oxygen atoms are in phase within the small terraces between consecutive missing rows but in antiphase between adjacent terraces [44].

In all cases, therefore, threefold sites appear to be the most stable sites for oxygen adsorption on the Rh(110) surface, even though stable structures where oxygen adsorbs in pairs in short bridge sites were evidenced at low coverage and low temperature [45, 46].

The situation is remarkably different when further oxygen is dosed on the $(2 \times 2)p2mg$-O structure at slightly lower temperatures (400–600 K). In this case a structure with (10×2) symmetry and high oxygen coverage forms, which is easily converted into the c(2×8)-O when the temperature is increased above 700 K [47], due to loss of oxygen for desorption or diffusion into the bulk. In figure 1(c) an STM image of the (10×2)-O surface is shown. It is characterized by a quite regular segmentation of the close-packed $[1\bar{1}0]$ metal rows, with segment ends almost aligned in the [001] direction, and by the presence of small, unreconstructed areas. In the inset, a zoom on the segments is presented. Each segment is composed on average by eight protrusions, with an internal distance 1/9 larger than the lattice constant, i.e. 3.0 Å instead of 2.7 Å. According to the model (see the figure), each protrusion represents a single rhodium atom and therefore the internal distance between adjacent protrusions is a measure of the surface strain. On both sides of the segments, oxygen atoms bind symmetrically in threefold sites, which, due to the strain, are more and more distorted towards the ends of the segments. The oxygen/surface rhodium atom ratio is therefore >2 (leading to an overall O coverage of 0.9 ML) and can be considered as a reason for the surface strain, which is relaxed by ejection of two out of ten metal atoms. The unreconstructed areas result from the condensation of the ejected Rh atoms and are covered by 1 ML of oxygen in the $(2 \times 1)p2mg$-O structure.

As already stated, all these structures require for their formation an elevated dosing temperature or a surface annealing after a low temperature exposure, indicating that this is an activated process.

In order to obtain O coverages higher than 1 ML using molecular oxygen, it is essential to work at high pressure: a recent paper by Dudin *et al* showed that when exposing the surface to O_2 at pressures in the range of 10^{-4} mbar and $T \sim 750$ K a surface oxide forms [48]. The morphology of the oxide film grown in O_2 ambient is complex, consisting of microscopic patches of different Rh and O atomic density, i.e. close to RhO_2 and Rh_2O_3. The authors proved that it is conversely possible to prepare a laterally uniform surface oxide in UHV by exposing the Rh(110) surface to atomic instead of molecular oxygen, thus excluding the O_2 dissociation step. The surface oxide has a c(2×4) periodicity and can be described as an O–Rh–O trilayer with a quasi-hexagonal arrangement of atoms in each layer. The Rh–Rh distance is reduced with respect to the Rh(110) substrate, leading to a metal density of 1.25 ML in the trilayer. Since there are two oxygen layers in the trilayer, the total O coverage is 2×1.25 ML.

2.2. *Interaction of nitrogen with the Rh(110) surface*

Formation of an ordered nitrogen overlayer on Rh(110) requires temperatures in the 430–480 K range and can be obtained either by NH_3 dissociation or by $NO + H_2$ reaction [32, 49–51]. Two ordered structures with (3×1) and (2×1) symmetries form at a coverage of $\sim$0.33 and 0.5 ML respectively. Both these structures involve an $(n \times 1)$ missing row reconstruction of

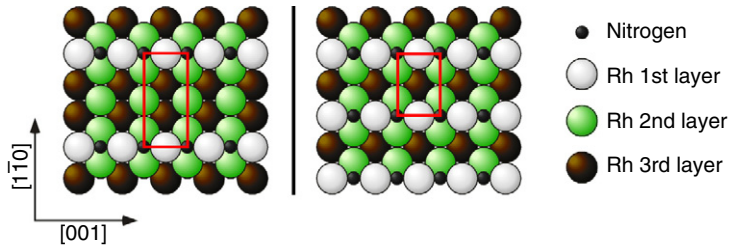

Figure 2. Models of nitrogen structures on Rh(110). Left, (3 × 1)-N; right, (2 × 1)-N.

the substrate, with Rh–N–Rh chains along the [001] direction, separated by two or three lattice constants in the [1$\bar{1}$0] direction. Nitrogen atoms sit in long bridge sites (see figure 2) [52–54].

2.3. Comparison with other transition metal fcc (110) surfaces

Several transition metal (TM) fcc (110) surfaces undergo reconstruction upon oxygen adsorption [4]. In particular, Cu(110), Ni(110) and Ag(110) exhibit (n × 1) reconstructions with added Me–O rows elongated in the [001] direction [55]. These reconstructions, therefore, differ substantially from the structures induced by oxygen on Rh(110) but closely resemble those induced by nitrogen on the same surface, with adsorbates sitting in long bridge sites between metal atoms in added chains. Conversely, O adsorption on Pd(110) results in missing row reconstructions where [1$\bar{1}$0] metal rows are removed and O atoms occupy threefold sites in a *zigzag* fashion along the remaining Pd rows [56, 57]. This is the same 'building block' as found on the Rh(110) surface, which points to a comparable oxygen–metal interaction for the two substrates.

In the case of other transition metals, such as Pt, Au and Ir, the clean surface is already reconstructed but it can undergo further rearrangement upon oxygen adsorption. In particular, on the Pt(110) surface, which is (1 × 2) reconstructed in its clean state, high coverage oxygen adsorption leads to a (12 × 2)-O structure very similar to the (10 × 2)-O structure on Rh(110) [58]. Indeed, both structures are characterized by the presence of strain along the close-packed metal rows, which leads to a quite regular segmentation, with two missing metal atoms, and by adsorption of O atoms in threefold sites on both sides of the metal ridges, so that each metal surface atom is coordinated with four oxygen atoms.

3. Surface reactions on Rh(110)

Surface reactions on Rh(110) have been extensively studied by STM in the last ten years. Two approaches have been used: either different amounts of reactant species have been deposited on the surface, which has subsequently been monitored by STM, or measurements have been performed during exposure. Both methods can give detailed information on the morphology of the surface during the reaction and on reaction mechanisms but in all cases a complete understanding of the processes requires combination with information from other techniques or from theory. For this reason, in the following description of STM studies of surface reactions, contributions from experiments by other techniques will be highlighted.

In this review we concentrate on reactions involving nitrogen and oxygen, which are not only important for real catalysis, but also allow us to demonstrate the capability of scanning tunnelling microscopy to study at the atomic scale processes such as surface restructuring, which are directly related to the reactivity. In particular, the attention is focused on two categories of reactions: dissociative adsorption and reactions of adsorbed oxygen layers.

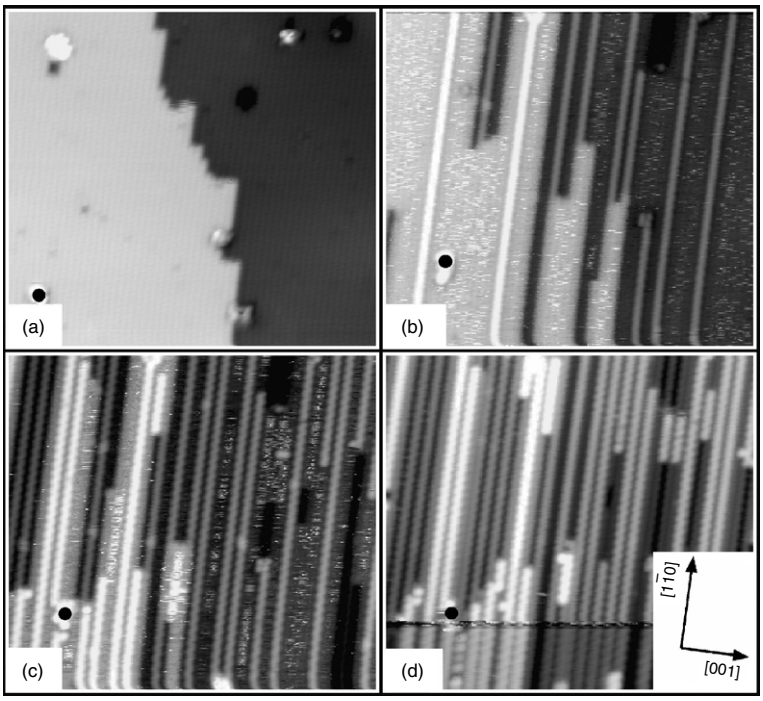

Figure 3. Oxygen dissociation. Sequence of STM images during exposure to molecular oxygen ($p_{O2} = 2 \times 10^{-10}$ mbar, $T = 390$ K): (a) clean Rh(110) surface; (b) mixed added + missing row reconstruction from step edges (1080 s after (a)); (c) troughs dug on the terraces (680 s after (b)); (d) $(2 \times 2)p2mg$-O surface (440 s after (c)). The black dot marks the position of the same defect in all images. (Image parameters: 20.5×18.6 nm^2, $V_B = +0.42$ V, $I = 1.29$ nA, 40 s/image.)

3.1. Dissociative adsorption on Rh(110)

Dissociative adsorption of molecules containing oxygen and/or nitrogen often involves a surface reconstruction, as highlighted in the previous section. The mechanism of this process involves events occurring at atomic scale, which makes the STM the instrument of choice.

In the following, the three cases of oxygen, nitrogen and competitive O/N dissociative adsorption will be presented, with an emphasis on the role of the induced surface reconstructions.

3.1.1. Oxygen. As described in section 2.1, oxygen adsorption at high temperature (∼400 K or above) induces a reconstruction of the substrate with missing rows in the [1$\bar{1}$0] direction. A detailed STM study, investigating the dynamics of this process [59], followed previous spectroscopic measurements [60].

Real-time high-resolution x-ray photoelectron spectroscopy (XPS) measurements during exposure of the surface to molecular oxygen at 570 K revealed that the O 1s spectrum of atomic oxygen is peaked at a binding energy of 529.95 eV at coverage below 0.1 ML, while an abrupt shift to 530.25 eV occurs above 0.1 ML [60]. The 530.25 eV O 1s peak corresponds to oxygen atoms adsorbed in threefold sites. It characterizes the adlayer until saturation, indicating that all adsorbed O atoms are involved in the growth of Rh–O chains. The adsorption site of O atoms at low coverage has not been determined but the authors suggest that the 529.95 eV peak stems from Rh–O nuclei formed when the O adatoms trap Rh atoms released by the onset of surface reconstruction, and the STM results described below further corroborate this hypothesis.

By STM imaging it was possible to follow the adsorption process during continuous O_2 exposure at 390 K [59]. The step edges of the clean surface (figure 3(a)) are not stable at 390 K, as metal atoms are seen to detach and attach in an even balance between subsequent images. This dynamics changes with the introduction of oxygen: the number of detaching Rh atoms significantly increases, leading to almost squared steps with borders aligned along either the [001] or the $[1\bar{1}0]$ direction. Concomitantly, bright dashes (BDs) appear, homogeneously distributed over the images. Their height is comparable with that of rhodium atoms, so they were interpreted as diffusing Rh–O units, temporarily intercepted by the STM tip.

The first stage of the oxidation is hence characterized by an O-induced detachment of Rh atoms from the step edges and a long-range mass transport in Rh–O units, which condense in added rows starting from defects, mainly step edges. As soon as new Rh atoms in added rows are imaged, they already have a *zigzag* appearance, indicative of oxygen atoms sitting in alternate threefold sites, as in the $(2 \times 2)p2mg$-O structure. When the coverage is about 0.1 ML, the detachment of kink atoms is substantially reduced and missing rows are dug starting from step edges to provide further Rh atoms. The reconstruction proceeds thus with a mixed missing + added row mechanism (see figure 3(b)).

When the reconstruction has already involved a large part of the surface, the rhodium atom supply from steps is greatly diminished—only a few missing rows can still be dug—and the long range mass transport is limited—only a few new Rh–O units are created and their diffusion is slowed down on the reconstructed surface. At this point another, local, reconstruction mechanism sets in: troughs are created on the terraces and the ejected atoms condense at their borders in $[1\bar{1}0]$ chains, which always appear in *zigzag*, i.e. they are immediately decorated by oxygen in threefold sites (figure 3(c)).

The reaction stages described above lead to the formation of a $(2 \times 2)p2mg$-O structure, which is actually not well ordered at the investigated temperature (390 K), as can be seen in figure 3(d). Further oxygen exposure at this temperature results in the formation of the metastable (10×2)-O structure. Additional oxygen atoms adsorb in the free threefold sites along the first layer metal rows, leading to a loss of *zigzag* appearance. Once a critical coverage of inserted oxygen is reached, rhodium atoms are ejected from the rows, thus creating the characteristic segmentation of the final structure. The ejected atoms diffuse along the missing rows until they nucleate in small unreconstructed areas randomly distributed on the surface. The length of the segments and their alignment are initially irregular and only in later oxidation stages does the order increase towards a (10×2) periodicity.

In conclusion, the O induced reconstruction is characterized by a strong interaction of oxygen atoms with step metal atoms. The main mechanism implies erosion of the steps, inducing a missing row restructuring. Only at a later stage are Rh atoms ejected directly from the terraces. During the whole process, the removed atoms condense in added rows, which grow starting from step edges.

It is interesting to compare the reconstruction mechanism induced by oxygen on the Rh(110) surface with those observed on other transition metal surfaces, such as Cu(110) [55], Ni(110) [61] and Ag(110) [62]. As stated in section 2.3, on these surfaces no missing rows are created but added Me–O chains form. Similarly to the case of rhodium, two different reconstruction mechanisms are present: (i) metal atoms are released from the steps; (ii) troughs are dug on the terraces. The weight of the two mechanisms depends on the specific substrate: while on Cu mechanism (i) predominates and mechanism (ii) comes into play only at later reconstruction stages, similarly to the case of Rh, on Ni the two processes compete from the beginning. Finally, on Ag, only mechanism (i) was found. In all the cases mentioned above, the removed metal atoms diffuse on the terraces until they condense with oxygen in added rows.

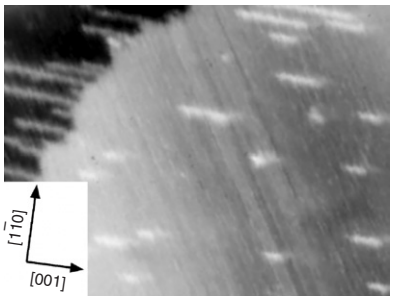

Figure 4. Ammonia dissociation. STM image acquired after exposure at 430 K, showing [001] oriented added Rh–N strings mainly starting at step edges.

This takes place homogeneously all over the surface and not only at step edges as occurs on the Rh surface.

3.1.2. Ammonia. We present now a study on ammonia adsorption, where N-driven missing row reconstructions set in.

The clean Rh(110) surface has been exposed to NH_3 at 430 K and the resulting structures have been investigated by LEED and STM [52]. A previous TPD/LEED/AES (Auger electron spectroscopy) study evidenced that NH_3 dissociates and hydrogen desorbs at $T \leqslant 400$ K [50], leaving pure N layers behind. LEED initially shows faint streaks in the [1$\bar{1}$0] direction followed by the development of streaky (3×1) and (2×1) patterns with increasing N coverage, indicating incomplete $(n \times 1)$ reconstructions. This is confirmed by STM images, which show bright Rh–N strings, elongated in the [001] direction, like the ones in figure 4: as the coverage increases, first strings of various lengths with large separation appear, followed by longer chains separated by three or two [1$\bar{1}$0] lattice constants. Even at high exposure, (3×1)-N and (2×1)-N islands coexist with areas where the density of chains is lower.

Concerning the reconstruction mechanism, step edges seem to be the main source of metal atoms. The condensation in added rows is apparently controlled by the mobility of Rh atoms: a lower concentration of Rh–N chains (bright strings) is present on the terraces with respect to the steps, as can be seen in figure 4, indicating that steps are the preferred nucleation centres. A minimum length of three Rh atoms is required for the nucleation of Rh–N rows.

In conclusion, similarly to oxygen, nitrogen preferentially interacts with metal atoms at steps, but while oxygen induces a mixed missing + added row reconstruction, N induced reconstruction is of added row type, i.e. no missing rows are dug from step edges. This difference might be traced back to the fact that while in the case of oxygen the metal/adsorbate chains are oriented in the [1$\bar{1}$0] direction, Rh–N chains are elongated in the [001] direction. In order to dig missing rows, therefore, nitrogen should break the close-packed rows, which is most likely energetically unfavourable.

3.1.3. Nitrogen monoxide. NO dissociation is another surface reaction representing the earlier STM studies on the Rh(110) surface [63, 64]. As already reported above, oxygen and nitrogen induce missing/added row surface reconstructions in the [001] and in the [1$\bar{1}$0] directions respectively, thus NO dissociation is an example of competitive restructuring.

In STM experiments, the sample was exposed to NO at 400 K to avoid molecular coadsorption, and quenched to room temperature (RT) before measuring [63]. At low coverage ($\sim$0.3 ML), a (3×1) LEED pattern with streaks in the [001] direction suggests the onset of

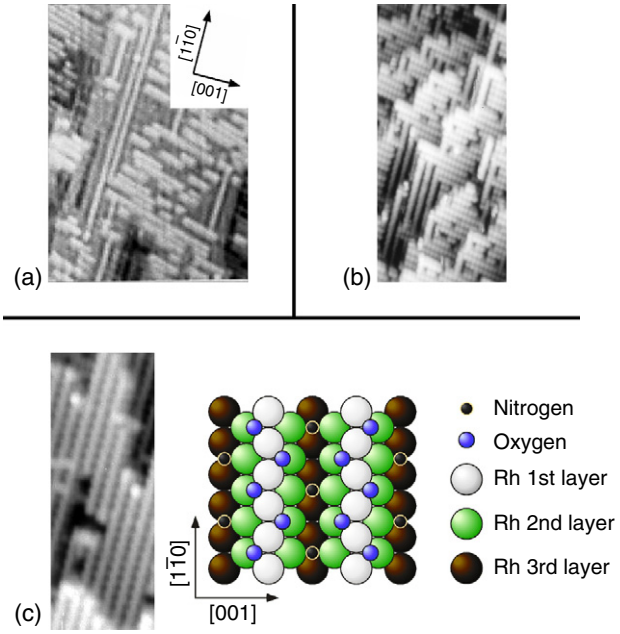

Figure 5. Nitrogen monoxide dissociation. STM images acquired after exposure at 400 K: (a) N + O layer (∼0.2 ML) where (3 × 1)-N islands dominate and only a few long Rh–O chains in the [1$\bar{1}$0] direction are present; (b) N + O layer (∼0.5 ML) where (2 × 1)-N and (1 × 2)-O reconstructed islands coexist; (c) N + O layer of c(2 × 4)-N + O structure with corresponding structural model.

an N-driven reconstruction, confirmed by STM observations (see figure 5(a)): islands of [001] oriented Rh–N chains with a preferred separation of three [1$\bar{1}$0] lattice constants dominate the images but [1$\bar{1}$0] oriented fairly long Rh–O strings are also present. These strings are longer than the [001] elongated chains; nevertheless, their spacing is random, which leads to the streaks in the LEED pattern. The length and the number of the rows indicate a comparable nucleation and growth rate for Rh–N chains, in contrast to the fewer but longer Rh–O chains, that points to a growth rate higher than the nucleation rate in the latter case. Rough estimations indicated that almost all N atoms participate in the formation of chains, while only a small fraction of O atoms is involved in Rh–O chains. The remaining oxygen is suggested to be disordered on the surface or to have penetrated subsurface.

At N + O coverage ∼0.5 ML, N- and O-driven reconstructions involve similar fractions of the surface: as shown in figure 5(b), the surface is equally shared between (2 × 1)-N and (1 × 2)-O islands, indicating a ∼0.5 ML local coverage both for nitrogen and for oxygen. (2 × 1)-N islands are smaller than (3 × 1)-N islands at ∼0.3 ML, pointing to a compression of Rh–N rows due to growing (1 × 2)-O islands that compete for a surface area. The Rh–O chains grow fast along the close packed direction, causing segmentation and shortening of the Rh–N rows.

When the coverage is further increased, a c(2 × 4) LEED pattern appears and STM images of the surface show a (1 × 2) reconstruction of the substrate, with long [1$\bar{1}$0] *zigzag* chains (see figure 5(c)). This structure is still a mixed N + O overlayer: oxygen removal by reaction with CO results in a (2 × 1)-N layer, while N desorption leads to a (2 × 2)*p*2*mg*-O layer. Images of the (2 × 2)*p*2*mg*-O and the c(2 × 4)-N + O structures differ only in the relative phase between adjacent rows: in phase for the pure oxygen layer, in antiphase for the mixed layer, due to the presence of nitrogen adatoms. As unambiguously determined by LEED I/V results [54], N atoms sit in long bridge sites (see the model in figure 5(c)).

Dynamical measurements provided further information about the initial stages of the reaction [64]. In this study the images were acquired during NO exposure while the sample slowly cooled down to room temperature. At very low coverage, the nucleation and growth of Rh–N units take place mainly on the terraces, where troughs are dug in the [001] direction to make Rh atoms available in adjacent areas. Only in regions close to steps are metal atoms supplied by the step edges, which increase their roughness at higher coverage. The observed behaviour indicates that the presence of oxygen changes the mechanism of the N-induced reconstruction from added-row type starting from the step edges [52] (see section 3.1.2) to a mixed missing/added-row mechanism, as in the case of O induced reconstruction (see section 3.1.1). This fact indicates that the steps have higher affinity for oxygen than for nitrogen. The nucleation of Rh–O rows starts later and their growth occurs preferentially from step edges, thus one layer below added Rh–N rows.

The transition from a N-driven (3×1) reconstruction to an O-driven (1×2) reconstruction proceeds via the intermediate state of coexisting (2×1)-N and (1×2)-O islands. Careful analysis of the images suggested a short range mass transport for the conversion to the c(2×4)-N + O structure which starts from the edge of the (2×1)-N islands.

3.2. Reactions of adsorbed oxygen layers on Rh(110)

Most of the catalytic surface reactions involve adsorbed species. Often the adsorbed species are one of the reactants and are exposed to the other reactant in the gas phase. For model system studies, this approach is particularly suitable when the substrate has a strong propensity to reconstruct, such as in the case of Rh(110), as it makes it possible to start from a well defined situation, where the surface structure is very well characterized.

Among the reactions on adsorbed layers, those involving oxygen have deserved special attention since they are of particular interest for oxidative catalysis, due to the high affinity of rhodium for oxygen and to the fact that oxygen is very often present in relevant surface reactions. Several studies addressed the reactivity of oxygen adlayers on Rh(110) exposed to gases that undergo oxidation.

In the following, three different oxidation reactions, involving carbon monoxide, ammonia and hydrogen respectively, will be presented.

3.2.1. Carbon monoxide oxidation. Carbon monoxide oxidation to CO_2 is one of the most widely studied surface reactions [65, 66]. Its practical importance and simplicity have allowed fundamental issues of the catalytic phenomena to be tackled. On the Rh(110) surface this reaction has been experimentally investigated both with spectroscopic techniques [67] and with atomic scale microscopy [2, 68]. A more detailed understanding of the underlying reaction mechanisms has been possible with the help of theory [68].

In 1993, Leibsle *et al* presented the first STM images of the Rh(110) surface after exposure of a mixed c(2×6)/c(2×8)-O layer to CO at room temperature [2]. They evidenced the presence of blurred, bright stripes, starting at [001] step edges and limited by $[1\bar{1}0]$ missing rows, where the reaction is going on. The bright appearance was attributed to patches of clean or CO covered rhodium and the fuzziness to vibrating or translating CO molecules. Weighting the reacted areas corresponding to the different reconstructions, the c(2×8)-O structure was found to be six times more reactive than the c(2×6)-O. A mechanism that involves nucleation of the reaction at [001] step edges was proposed, as only there free Rh sites are available for CO adsorption. The reaction then propagates in a one-dimensional manner, in the $[1\bar{1}0]$ direction, along the narrow terraces between adjacent missing rows, which are typical of the c$(2 \times 2n)$-O structures.

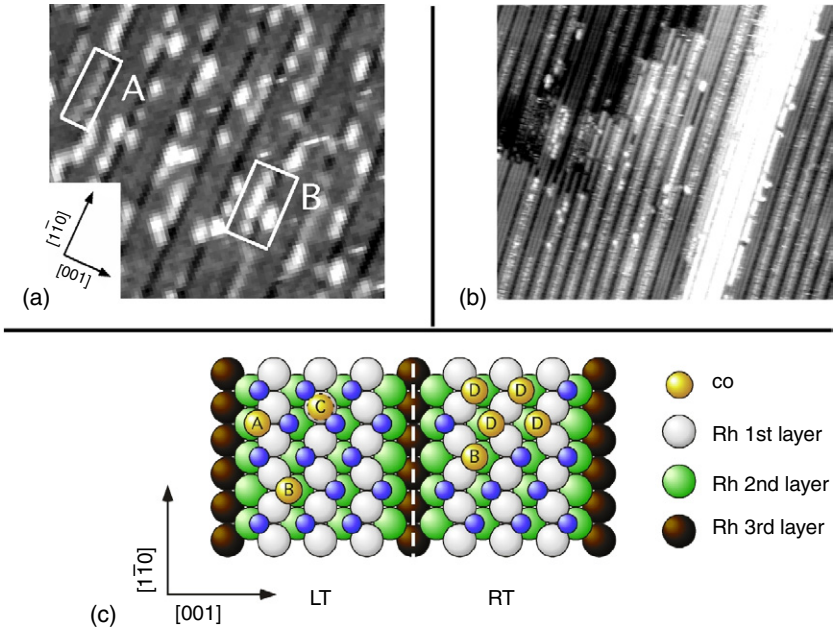

Figure 6. Carbon monoxide oxidation. (a) The reaction at low temperature. Two species of CO molecules are present. Patches of CO_A and CO_B are indicated. (b) The reaction at room temperature. 'Christmas garlands' form starting from step edges. (c) Structural model showing the different CO species present on the surface at LT (left) and at RT (right). (Image parameters: (a) 160 K, 16×14 nm^2, $V_B = -0.1$ V, $I = 1$ nA; (b) 300 K, 42×36 nm^2, $V_B = +0.5$ V, $I = 1$ nA.)

Later on, the CO oxidation on Rh(110) was an issue of other investigations. XPS measurements [67] indicated a vigorous reactivity of the c(2 × 8)-O structure at $T \geqslant$ RT. Conversely, if the exposure is carried out at 200 K, only 25% of oxygen is removed quickly and afterwards the oxidation rate levels off with a final O coverage of 0.36 ML remaining on the surface. At low temperature (LT) the ongoing reaction is accompanied by the appearance in the XPS spectra of a CO species not present at RT and strongly affected by the presence of co-adsorbed oxygen.

The XPS results suggest the existence of two different reaction mechanisms for the oxidation of the c(2 × 8)-O structure at RT and at 200 K. Indeed more recently a combined STM–density functional theory (DFT) study confirmed this hint [68]. After exposure of the c(2 × 8)-O surface to CO at 160 K, bright features attributed to CO molecules are present all over the surface, anywhere along the close-packed metal rows, in remarkable contrast with the mechanism found by Leibsle *et al* at RT. At LT, therefore, a distinct reaction pathway holds, which is quenched at higher temperatures. STM images coupled with DFT calculations allowed description of this reaction mechanism in detail. Two kinds of CO molecules are imaged, as shown in figure 6(a): a first species, CO_A, lies in chains, with double Rh–Rh distance periodicity, along the borders of the terraces (i.e. adjacent to the missing rows). These molecules sit in free threefold sites, without removing the initial oxygen atoms, which act as a template for CO adsorption. With nice agreement between experiments and theory, the CO_A molecules are slightly tilted towards the missing rows. A second species of CO molecules, named CO_B, appears brighter and is adsorbed on oxygen vacancy sites, mostly located towards the centre of the terraces. DFT calculations assigned to CO_B molecules a twofold adsorption site on the rhodium rows enclosing the terraces, slightly moved from the short bridge towards

the inside of the terrace. These findings are consistent with XPS results [67], since CO_A can be identified as the characteristic LT CO species strongly affected by co-adsorbed oxygen, while the presence of CO_B can explain the growth of a peak at a binding energy similar to the one of CO on the clean surface.

DFT calculations then allowed depiction of the complete LT reaction pathway. A third species of CO, CO_C, adsorbed on top of rhodium atoms on the fully oxygen covered terrace, exists as a mobile precursor at the investigated temperature. Three possible final states for CO_C molecules are possible: either they desorb, or move to the free threefold sites along the borders of the terraces and convert to CO_A without reacting, or they react with oxygen atoms in the middle of the terraces, thus creating free adsorption sites where further CO molecules adsorb as CO_B. The overall reaction can nucleate homogeneously on the surface but it stops working as the oxygen coverage decreases, since it requires a special configuration of three neighbouring oxygen atoms to proceed. Due to the short-lived nature of CO_C, only CO_A and CO_B molecules can be resolved in the images. The model in figure 6((c)—left) summarizes schematically the three CO species that are involved in the LT reaction mechanism.

At RT, instead, STM images by Castellarin-Cudia *et al* confirmed the results of Leibsle *et al*. The reaction nucleates at steps and propagates along the narrow terraces of the c(2 × 8)-O. CO molecules are not imaged sharply but have a spiky structure, resembling Christmas garlands, due to a strong interaction with the scanning tip (see figure 6(b)). Near the central line of the terraces, though, the molecules are better resolved, without any fuzziness, indicating a more stable CO adsorption site. These latter molecules are identified as a CO_D species in DFT calculations (see figure 6((c)—right)). The room temperature reaction mechanism is explained with the removal of oxygen atoms from the central metal rows at step edges. As soon as free adsorption sites are created, CO molecules adsorb as CO_D, which react with further central oxygen, and the reaction thus proceeds along the terrace. In the reacted areas, CO_D molecules have mostly CO neighbours, which explains the binding energy different from the one at LT (related to CO_B) observed in XPS measurements [67]. When all the central oxygen atoms are removed with this reaction mechanism, 0.25 ML of oxygen is left on the surface, in fair agreement with XPS data [67].

The quenching of the LT reaction pathway at higher temperatures can be explained by the short lifetime of the CO_C species.

3.2.2. Ammonia oxidation. The ammonia oxidation reaction is a case of a reaction where the final structure of the surface layer is determined by the final reaction products, since it leads not only to the formation of water, which immediately desorbs, but also of nitrogen atoms, which stay on the surface. In a combined STM/LEED/XPS/TPD study, Kiskinova *et al* investigated the reaction on the Rh(110) surface starting from a c(2 × 8)-O layer [69]. The transition from the O-driven to the N-driven phase was found to occur through an intermediate metastable surface phase that cannot be formed by either of the reaction participants alone.

The reaction was carried out at 380 K and the sample was subsequently cooled down to 300 K. According to the reaction stoichiometry, $2NH_3 + 3O_{ad} = 3H_2O_g + 2N_{ad}$, after complete removal of oxygen, 0.5 ML of N remains on the surface, which, at slightly higher temperatures, should lead to a (2 × 1) reconstruction of the substrate (see section 2.2). However, after the reduction the LEED experiments showed a weak c(2 × 6) pattern and XPS and TPD experiments confirmed that only nitrogen is present on the surface. Corresponding STM images showed that the flat terraces are covered by short segments, elongated in the [001] direction, consisting of three bright protrusions, as shown in figure 7. Line profiles along the segments revealed that their length is consistent with the presence of three Rh atoms, while profiles across the segments showed a corrugation consistent with a (2 × 1) reconstruction. The

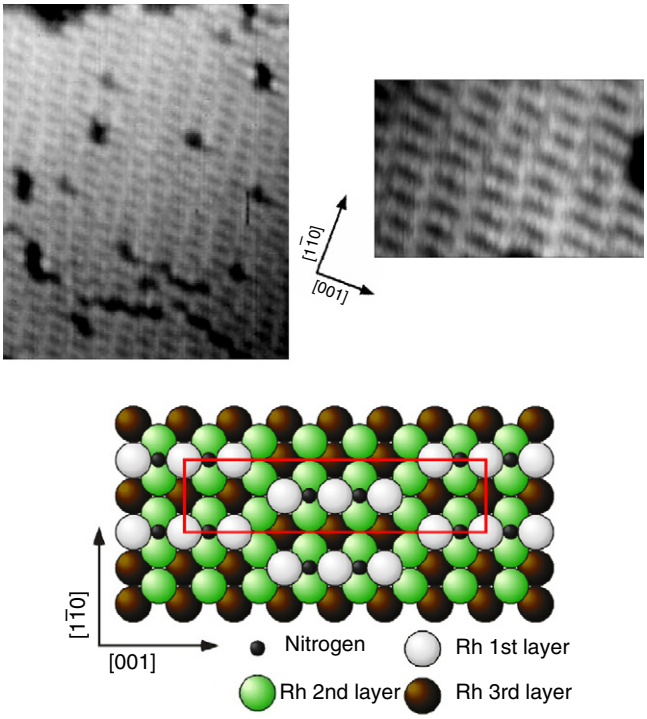

Figure 7. Ammonia oxidation. STM images acquired after exposure of the c(2 × 8)-O surface to NH_3 at 380 K and corresponding structural model. The intermediate c(2 × 6)-N structure, made of a long range quasi-hexagonal arrangement of trimers, is better resolved in the image on the right. Delocalized N atoms, supposed to be present in the region between trimer edge Rh atoms (according to [69]), are not indicated in the model.

trimers are arranged in the [1$\bar{1}$0] direction in a *zigzag* fashion, thus leading to a quasi-hexagonal superlattice and a c(2 × 6) symmetry.

It is remarkable to note the similarity between the Rh–N trimer structure and the segmented Rh–O structures, i.e. the (10 × 2)-O (described in section 2.2) and the structures in mixed K + O adlayers [70]. In particular, the c(2 × 6)-N structure resembles the c(8 × 2)-K + O structure that is formed by oxidizing the Rh(110) surface in the presence of potassium, except for the orientation of the segments: along the [001] direction in the c(2 × 6)-N and along the [1$\bar{1}$0] direction in the c(8 × 2)-K + O. This prompts a general tendency for the Rh(110) surface to form intermediate, metastable structures involving a segmentation of the topmost metal layer. The direction of the segments is determined by the reconstructive action of the adsorbates, i.e. along the [001] direction for N–Rh segments and along the [1$\bar{1}$0] direction for O–Rh segments.

Annealing the trimer layer to 450 K resulted in a (2 × 1)-N structure without any loss of nitrogen, as confirmed by XPS and TPD experiments. This indicates that the trimer structure mediates the conversion from the O-driven (1 × 4) reconstruction to the N-driven (2 × 1) reconstruction.

A tentative explanation of the conversion mechanism has been proposed by the authors. The initial (1 × 4) reconstructed substrate constrains the reaction within each group of three top-layer rhodium rows, which will later originate the trimers. After complete oxygen removal, a c(2 × 6)-N structure forms, consisting of [001] trimers arranged in a quasi-hexagonal superstructure.

The final structure, therefore, carries memory of the original (1×4) reconstruction but the local geometry is severely changed.

Further conversion to the (2×1)-N structure involves a shift of the trimers in the $[1\bar{1}0]$ direction, which requires overcoming an activation barrier, for example by raising the temperature to 450 K.

3.2.3. Hydrogen oxidation. Hydrogen oxidation has been fully characterized on the whole sequence of O-induced surface structures [71–73, 48], which allows us to compare the reactivity of the different O adlayers. When an oxygen-covered surface is exposed to hydrogen, water molecules form and readily desorb, provided the reaction temperature is high enough (above 250 K on the clean surface). In some cases it has been possible, with the help of theory, to elucidate the mechanism of the formation itself; in other cases the focus was on the overall propagation of the reaction. The substrate preserves the reconstructed phase when the reduction of oxygen is carried out at $T < 400$ K. Nevertheless, these clean, reconstructed phases are only metastable and, at $T > 470$ K, they convert to the more stable (1×1) phase [41]. In some of the following studies, the reaction temperature was accordingly chosen, to allow the investigation of the deconstruction mechanism.

Since hydrogen does not interact strongly with the tip, on all oxygen covered Rh(110) surfaces dynamic STM measurements could be performed. The surface was kept at stable temperature and molecular hydrogen was let into the chamber while acquiring series of hundreds of STM images from the same area. Due to a screening effect of the tip, the effective gas pressure in the proximity of the surface is reduced by an estimated factor of five [59].

In this section, the various studies are presented starting from the O-saturated unreconstructed surface, where the water formation mechanism has been analysed more accurately. Afterwards, the reaction on the $(2 \times 2)p2mg$-O surface and the related $(1 \times 2) \rightarrow (1 \times 1)$ deconstruction will be addressed. The case of the (10×2)-O surface is more complicated, since the reaction proceeds in two steps and the help of theory turned out to be essential for a complete understanding. Finally, a brief discussion of the reduction reaction on the rhodium surface oxide will be given. At the end of the section, we highlight common trends and analogies between the various surfaces.

3.2.3a. $(2 \times 1)p2mg$-O. We start the discussion reporting a recent joint STM–DFT study on the water production reaction on the unreconstructed Rh(110) surface [71]. The starting layer consists of the saturated $(2 \times 1)p2mg$-O structure, where 1 ML of oxygen atoms sit in threefold sites in a *zigzag* fashion along the close-packed metal rows. A great deal of attention was devoted to the preparation of the structure, in order to obtain the best-ordered starting layer. It turned out that an initial reconstruction of the surface already sets in when exposing the clean surface to molecular oxygen at T in the 270–300 K range. Since the aim of the study was the investigation of the water formation reaction in conditions with no influence of surface restructuring, it was necessary to prepare the structure at lower T. Nevertheless, exposure at low T results in a $(2 \times 1)p2mg$-O structure where *chain-like* defects are present. The best result was obtained when the exposure was carried out at 200 K, followed by annealing to 260 K (see figure 8(a)).

This layer was then exposed to molecular hydrogen ($p_{H2} = 5 \times 10^{-9}$ mbar on the surface) at 260 K while scanning. The temperature has been chosen in order to allow the reaction to proceed on a suitable timescale. After a short induction period, a reaction front, clearly visible in figure 8(b), crosses the surface. The propagation of the wavefront requires an autocatalytic process: the H_2 dissociation is initially possible only at local defects (e.g. steps) while it occurs

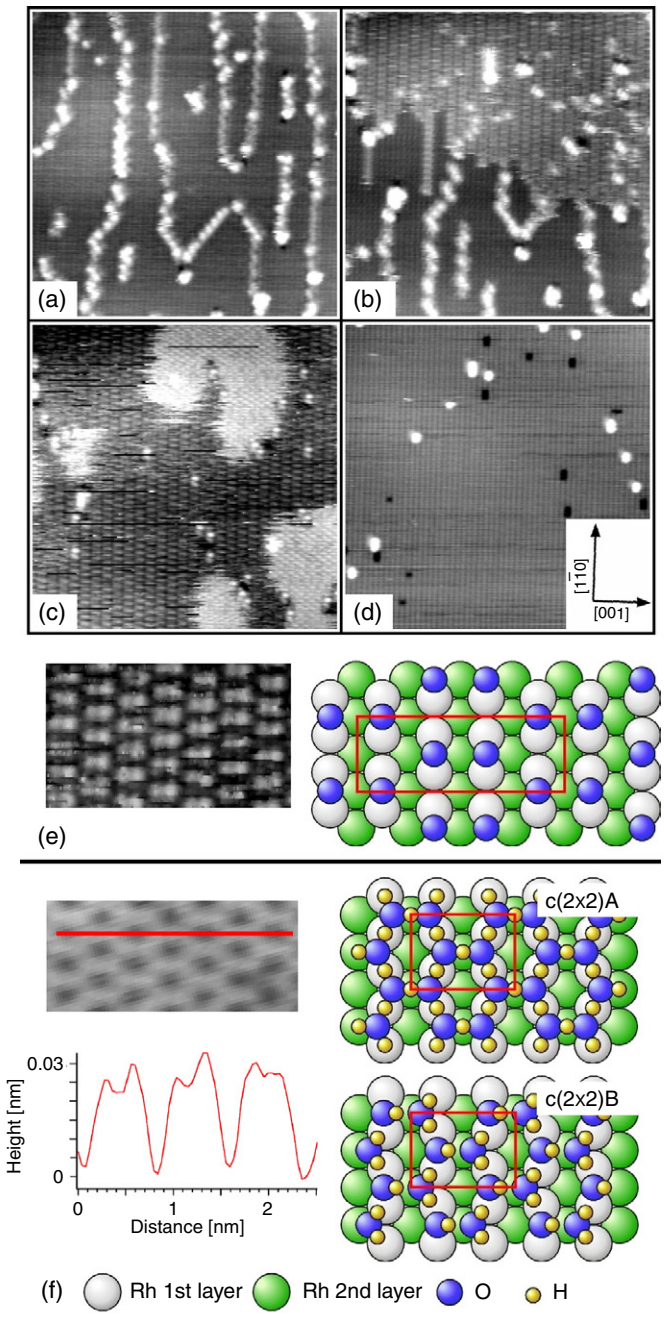

Figure 8. Hydrogen oxidation on the $(2 \times 1)p2mg$-O surface. ((a)–(d)) Sequence of STM images during exposure to molecular hydrogen ($p_{H2} = 5 \times 10^{-9}$ mbar, $T = 260$ K). (a) Initial surface. (b) Reaction front crossing the surface. Behind the front a $c(2 \times 4)$ structure forms (630 s after (a)). (c) Islands of intermediate $c(2 \times 2)$ structure (175 s after (b)). (d) Final, clean, surface (875 s after (c)). (e) Atomically resolved STM image and model of the $c(2 \times 4)$-O structure. (f) Atomically resolved STM image, line profile (along red line), and two alternative models of the intermediate $c(2 \times 2)$ structure. (Image parameters: (a)–(d) 27×27 nm^2, $V_B = +0.14$ V, $I = 1.58$ nA, 35 s/image; (e) 55×32 nm^2, $V_B = +0.13$ V, $I = 1.02$ nA; (f) 24×18 nm^2, $V_B = +0.46$ V, $I = 0.59$ nA.)

behind the front, where free sites on the terraces are created, as soon as the reaction starts propagating.

Behind the reaction front a new structure, composed of pairs of bright protrusions in a c(2 × 4) arrangement, immediately forms (see figure 8(e) for a zoom on this structure). Comparison with previous STM measurements, which evidenced the existence of pairs of oxygen atoms in short bridge sites at low T [45], suggested that the c(2 × 4) structure is due to a rearrangement of oxygen after the removal of a fraction of the initial coverage. This hypothesis has been confirmed by DFT calculations, which found it to be a stable structure, and by related simulated STM images, which nicely reproduce the experimental ones. As further evidence, the same layer has been prepared on the clean surface by dosing a lower amount of O_2 at the reaction temperature. In the c(2 × 4)-O structure, 0.5 ML of oxygen atoms sit in short-bridge sites, as illustrated by the model in figure 8(e), despite the reduced O–O distance imaged by STM, which is an electronic and not a topographic effect [45, 46].

On the c(2 × 4)-O surface, the reaction proceeds following a new pathway that includes compression of the dilute O layer. Islands of an intermediate c(2 × 2) structure, appearing brighter in the STM images, nucleate on the terraces at local defects (see figure 8(c)) and grow at the expense of the c(2 × 4)-O structure up to a maximum extension that covers about half of the surface. Afterwards, the islands decay, reducing their size from the borders, and a clean Rh(110) substrate is restored (figure 8(d)). The c(2 × 2) structure has a quasi-hexagonal arrangement (see figure 8(f)) and, as a distinctive characteristic that has been crucial for the identification of the structure, it appears in STM line-scans as composed of double-peak features.

It is clear that hydrogen is present in the compressed layer but it has not been possible to propose a unique atomic description for the c(2 × 2) structure. Two alternative models, which can be seen in figure 8(f), have been proposed. The first model, named c(2 × 2)A, is an O + H coadsorption layer, where 1 ML of oxygen atoms sit in a *zigzag* fashion along the close-packed metal rows in antiphase between adjacent rows, so that a quasi-hexagonal O arrangement results. 1.5 ML of hydrogen atoms bridge neighbouring O atoms in pairs, with only a weak interaction with the substrate. As a consequence, a quasi-hexagonal hydrogen bond network results. The second model for the c(2 × 2) structure, named c(2 × 2)B, involves a mixed OH–H_2O layer, similarly to the half dissociated water layers found on Ru(0001) [74] and Pt(110) [75]. 0.5 ML of water molecules and 0.5 ML of OH groups are disposed in a quasi-hexagonal arrangement, interconnected by a hydrogen bond network. OH groups sit in roughly short-bridge sites with H pointing upwards to H_2O, while water molecules are placed farther from the surface, with O atoms above threefold sites and H pointing downwards to the OH groups. STM images have been simulated for both models but only c(2 × 2)A reproduces the double peaks in line-scans. Nevertheless, model c(2 × 2)B is much more stable than c(2 × 2)A and there is no barrier for the conversion from c(2 × 2)A to c(2 × 2)B, which might kinetically hinder its formation. The study was therefore not conclusive on the exact atomic description of the intermediate structure.

Regardless of the actual model of the c(2 × 2) structure, both hypotheses involve 1 ML of oxygen, either as single atoms or incorporated in molecules. This indicates that all oxygen atoms initially present on the surface in the c(2 × 4)-O structure (0.5 ML all over the surface) are included in the c(2 × 2) structure (1 ML local coverage on about half of the surface at the maximum extension). The c(2 × 4)-O phase is therefore unreactive at the investigated temperature and has to be converted into the reactive c(2 × 2) before the reaction can proceed. This conversion involves the formation of a hydrogen bond network.

A complete scenario for the second part of the reaction can now be proposed. In the proximity of defects, hydrogen starts interacting with O atoms of the c(2 × 4)-O structure,

creating the first nuclei of the c(2 × 2) structure. Due to this condensation, free patches of metal substrate are created, where further O atoms from the c(2 × 4)-O can diffuse, as also shown in STM images. As soon as O atoms get close to a c(2 × 2) nucleus, they are trapped in the hydrogen bond network and the island grows. When the conversion between the two phases is completed, further hydrogenation occurs at the island borders, where water molecules desorb.

3.2.3b. (2 × 2)p2mg-O. As an example of hydrogen oxidation on a missing row reconstructed surface, the exposure of the $(2 \times 2)\,p2mg$-O to H_2 has been investigated [72]. The exposure has been performed in the 380–405 K temperature range, which allows the deconstruction of the metastable (1 × 2) metal substrate after reduction of the oxygen layer, and ensures a timescale matching the time resolution of the microscope for the restructuring of the surface. The study can be divided into two parts: in the first part, the reaction itself has been analysed, while the second one focuses on the dynamics of the deconstruction of the clean (1 × 2) substrate, which starts after the reaction and develops on a timescale about 40 times slower.

Concerning the reaction mechanism, previous photoemission electron microscopy (PEEM) studies under steady-state conditions tackled the reduction of an oxygen saturated Rh(110) surface by hydrogen in the 480–780 K temperature range [76, 77]. Initiated by defects, the reaction was found to proceed via an elliptical reaction front. The anisotropy of front propagation changes drastically depending on the experimental parameters. It has to be noted, though, that in the PEEM experiments the starting surface was not a well ordered structure but a mixture of reconstructed phases.

STM image series have been acquired while exposing the $(2 \times 2)\,p2mg$-O surface (figure 9(a)) to hydrogen with $p_{H2} = 2 \times 10^{-8}$ mbar (corrected for the tip screening factor). In agreement with the PEEM results, despite the different starting structure and the 100 K lower temperature, the reaction was seen to propagate via a reaction front that appears as finger-like structures in the STM images, after nucleation at steps. The front is markedly anisotropic, mainly elongated in the missing row direction. On smaller scale images, the ongoing reaction is evidenced by the appearance of bright dashes constrained on the metal rows (see figure 9(b)). In a second stage, a contrast reversal occurs, with dark dashes on brighter metal rows (see figure 9(c)). The dark dashes then become less and less wide and gradually disappear. The bright dashes have been associated with diffusing oxygen vacancies and the dark dashes with diffusing oxygen atoms. Based on such identification, the propagation of the reaction can be explained by the initial removal of a few oxygen atoms, which leave behind a few oxygen vacancies. The vacancies are mobile (i.e. O atoms can jump into the vacancies from neighbouring $(2 \times 2)\,p2mg$-O parts of the row), cluster and increase their number as the reaction proceeds, until only a few O atoms remain on the rhodium rows. These remaining O atoms diffuse on the almost O free rows with a diffusion constant similar to that of the vacancies. Finally, a clean (1 × 2) surface is produced.

Conversely to the STM study of hydrogen oxidation on the $(2 \times 1)\,p2mg$-O, unreconstructed Rh(110) surface (see section 3.2.3a), no intermediate reaction products have been resolved, due to the higher reaction temperature, which allows a fast reaction and the immediate desorption of water.

The deconstruction of the (1 × 2) substrate in the 400–500 K temperature range had been previously investigated by He atom scattering (HAS) [78]. Cvetko *et al* found that the transformation takes place by the formation of (1 × 1) islands elongated in the $[1\bar{1}0]$ direction. The surface remains flat, with terraces distributed over only two height levels, so that a monatomic step *down* necessarily follows a step *up*. The authors suggest a deconstruction mechanism based on the pairing of rhodium rows, leading to areas where two metal rows in the upper level are next to two metal rows in the lower level, with an overall (1 × 4) symmetry.

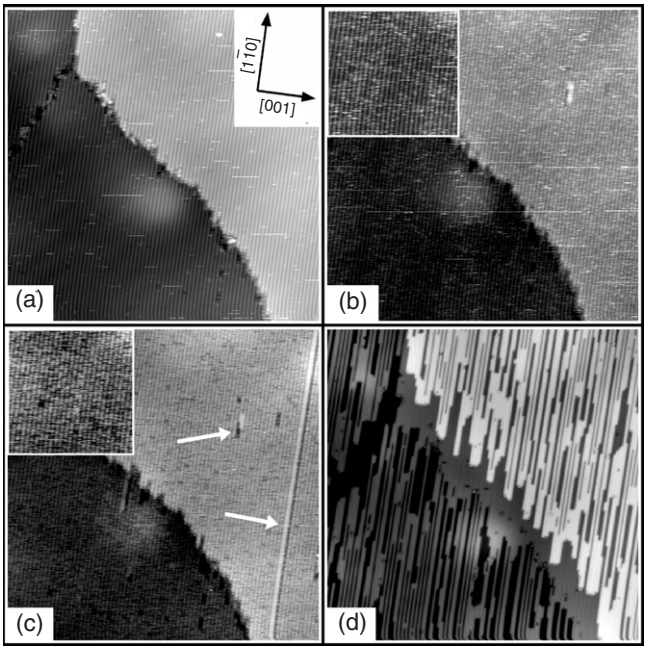

Figure 9. Hydrogen oxidation on the $(2 \times 2)p2mg$-O surface. Sequence of STM images during exposure to molecular hydrogen ($p_{H2} = 2 \times 10^{-8}$ mbar, $T = 390$ K). (a) Initial surface. (b) Ongoing reaction. Bright dashes constrained on the metal rows, better resolved in the inset (132 s after (a)). (c) Ongoing reaction. Dark dashes constrained on the metal rows, better resolved in the inset. Beginning of the deconstruction process. The arrows indicate the two different deconstruction mechanisms: holes with neighbouring (1×1) islands, formed by the ejected atoms, and row pairing (352 s after (b)). (d) Deconstructed surface. Areas created by step retraction can also be seen (2 h 37 min after (c)). (Image parameters: 60×60 nm^2, $V_B = +0.42$ V, $I = 1.32$ nA, 44 s/image; insets: 20×20 nm^2.)

STM time series confirmed the row-pairing mechanism proposed in the HAS experiments, as shown in figure 9(c). At later stages, even row triplets form, where a (1×2) row couples with a two-row *up* terrace, but then the pairing mechanism stops, i.e. double missing rows are not crossed in the deconstruction process. Indeed also in HAS measurements it was necessary to raise the temperature from 400 to 500 K to let the deconstruction proceed with the coalescence in larger (1×1) terraces. Nevertheless, a second deconstruction mechanism was evidenced by STM and significantly contributes to the evolution towards a (1×1) surface. Single atoms detach from the (1×2) rhodium rows, thus creating holes, which expose (1×1) *down* areas of the underlying layer (see figure 9(c)). The ejected atoms diffuse along the missing rows until condensing in small (1×1) *up* islands. Further ejected rhodium atoms diffuse in the missing rows but they are blocked by the *up* islands, which therefore grow in the direction of the holes. Pairs of *up* and *down* terraces of approximately the same extensions are thus created. This second mechanism is of local nature and does not lead to a particular symmetry; therefore it can hardly be detected with non-local techniques. When the detachment of single atoms occurs at step edges, the deconstruction mechanism leads to a retraction of the steps (see figure 9(d)), which unravels large unreconstructed patches of the underlying layer. The ejected atoms diffuse exclusively in the missing rows of the upper terrace and their condensation into islands prevents a further retraction of the steps. Both deconstruction mechanisms start mainly at defects, which indicates that a perfect (1×2) surface would probably not deconstruct. In the

investigated temperature range the final surface always presents the coexistence of limited *up* and *down* terraces, as evidenced by the image in figure 9(d), and an annealing of the surface to higher T is necessary to obtain a well ordered (1×1) surface, with large terraces.

A recent joint high-resolution core-level spectroscopy and DFT study confirmed the role of defects in the first stages of the deconstruction process, thus supporting the previous STM observations [79], even though the pairing mechanism was not favoured by the DFT calculations.

3.2.3c. (10×2)*-O.* In moving towards high local O coverage structures, which are potentially relevant as intermediates for the surface oxide formation, the (10×2)-O structure represents an important intermediate, since metal atoms are highly coordinated to O and start to move out of registry. The investigation of the hydrogen oxidation reaction on the (10×2)-O surface allows us, therefore, to address questions on the influence of strain and segmentation on the reactivity of a surface. As described in section 2.1, in fact, the (10×2)-O structure is characterized by an 11% strain along the close-packed $[1\bar{1}0]$ metal rows on the (1×2) reconstructed Rh(110) substrate. Due to the strain, two out of ten rhodium atoms are ejected from the rows, leading to a segmentation of the surface, with segments separated by ridge vacancies, quite well aligned along the [001] direction.

After starting exposure of the (10×2)-O surface to molecular hydrogen ($p_{H2} = 1 \times 10^{-8}$ mbar on the surface) at RT, the STM images reveal a reaction front that propagates across the surface (as indicated in figures 10(a)–(c)) [73]. Close inspection evidenced that the reaction does not nucleate on segmented areas of the surface but on wide unreconstructed regions, which are intrinsically part of the surface, mainly at step edges but sometimes also in the middle of a terrace, and only from these regions does it propagate to the segmented islands starting from their border, as shown in the sequence of STM images in figures 10(a)–(c). The hydrogen dissociation barrier and the OH formation barrier at segmented island edges, in the troughs at segment middle parts, and at ridge vacancies have been calculated by DFT. Indeed, the calculations confirmed the experimental findings, since the barriers were found to be much smaller at segmented island edges, where a sufficiently large ensemble of clean Rh atoms is present.

Going into the details of the reduction, on the wide unreconstructed regions, which are initially covered by the $(2 \times 1)\,p2mg$-O structure, the reaction proceeds exactly as on the pure $(2 \times 1)\,p2mg$-O unreconstructed Rh(110) surface, with a wavefront removing half of the initial oxygen atoms and leaving behind a c(2×4) arrangement of the remaining atoms. Once the reaction front crosses the whole unreconstructed area, it attacks the segmented (10×2)-O structure, where it continues its propagation without being affected by the presence of steps or other defects. At the investigated temperature the front is clearly elliptical, elongated in the $[1\bar{1}0]$ direction.

On (10×2) areas, the passage of the reaction front removes only half of the initial oxygen coverage. The reaction propagates in a *zigzag* fashion along each segment, reducing one threefold O atom per couple, as shown in the sequence of images in figures 10(d)–(f) and clarified by the models in figure 10(g). DFT calculations attributed the *zigzag* propagation to thermodynamic effects: the lowest binding energy among the oxygen atoms adjacent to the first oxygen vacancy was indeed found for the O atom extending the *zigzag*. As soon as half of the oxygen is removed, the strain is locally relieved. At room temperature this strain removal induces a transient short-range mobility of Rh atoms, which results in an alteration of the initially regular superstructure of the segments, clearly visible in figure 10(f).

At the atomic scale, the propagation of the reaction front can thus be explained as due to the formation of new ensembles of less-oxidized rhodium atoms where further molecular hydrogen

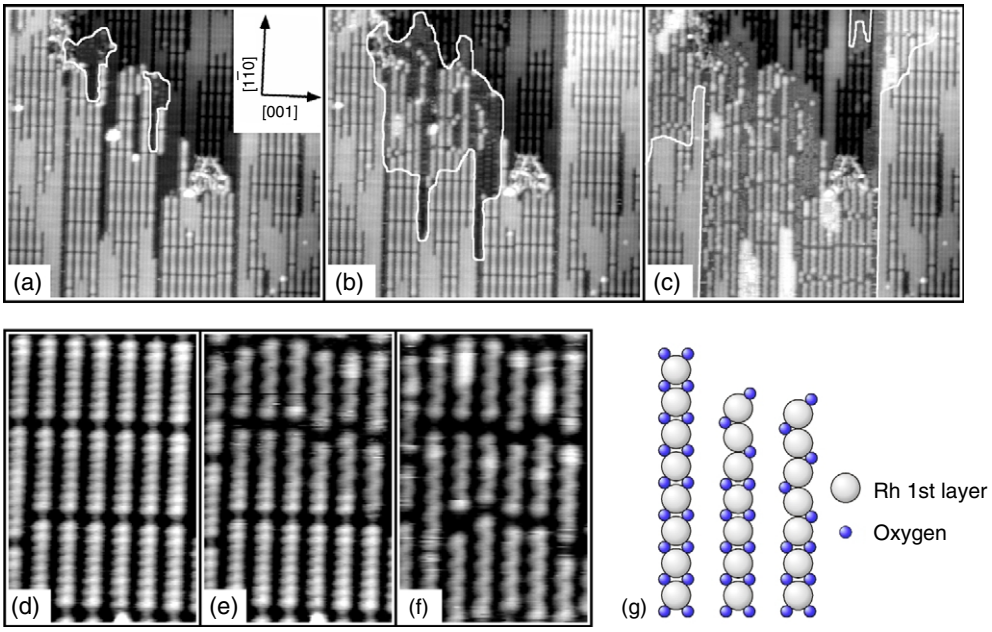

Figure 10. Hydrogen oxidation on the (10 × 2)-O surface. (a)–(c) Sequence of large-scale STM images during exposure to molecular hydrogen ($p_{H2} = 1 \times 10^{-8}$ mbar, $T = 300$ K). White lines mark the position of the reaction front. (a) Nucleation of the reaction on unreconstructed areas at step edges (770 s after starting exposure); (b) the reaction involves the whole unreconstructed area and starts propagating to the segmented (10 × 2) (140 s after (a)); (c) the reaction continues its propagation on the (10 × 2) surface (210 s after (b)). (d)–(f) Sequence of small-scale STM images during exposure, showing the details of the propagation of the reaction front along the segments, evidenced by the formation of a *zigzag*. When the second reaction step takes place, also the *zigzag* oxygen is removed and the segment appears locally brighter (time between images: 35 s). (g) Propagation mechanism of the reaction front along a single segment. Starting from a segment end, one out of two oxygen atoms is reacted off, proceeding in a *zigzag* fashion. As soon as an O atom is removed, the strain is locally released. (Image parameters: (a)–(c) 38 × 35 nm^2, $V_B = +0.64$ V, $I = 0.46$ nA, 35 s/image; (d)–(f) 6 × 10 nm^2, $V_B = +0.53$ V, $I = 0.86$ nA, 35 s/image.)

(This figure is in colour only in the electronic version)

can dissociate: on wide unreconstructed areas this is a consequence of the reorganization of O atoms in the c(2 × 4)-O structure, while on the (10 × 2) part of the surface it is related to a combination of the effects of strain and segmentation. As soon as the O coverage on the segments is reduced, in fact, the strain removal enlarges the ridge vacancies, thus exposing new patches of clean metal. The formation of free adsorption sites for hydrogen dissociation is therefore the autocatalytic step.

As described above, behind the reaction front, half of the initial oxygen atoms are still present. The reaction requires thus a second step to be completed. On the unreconstructed areas of the surface, the process continues by the nucleation of c(2 × 2) islands as on the pure (2 × 1)$p2mg$-O layer as soon as the front propagates to the segmented areas. On the segments, the second reaction step nucleates homogeneously all over the surface. Such a different behaviour has been confirmed by DFT calculations proving that H_2 dissociation occurs everywhere on the surface, in the enlarged ridge vacancies and in the (1 × 2) troughs. Nevertheless, STM results evidenced that the complete oxygen removal on each single segment can start only from the ridge vacancies and from these special active sites it propagates to the

middle part of the segment. Again DFT calculations corroborated the experimental findings, showing that H atoms can only adsorb in the enlarged ridge vacancies, from which OH formation takes place. With such a mechanism the reaction proceeds, more slowly than in the first reaction step, until a clean, segmented, (1 × 2) rhodium surface is produced.

The second reaction step on the (10 × 2)-O surface closely resembles the reduction reaction on the (2 × 2)$p2mg$-O surface (see section 3.2.3b and [72]), the only difference in the initial surface being the presence of the segmentation. Thus, by comparing the two systems it is possible to unravel in a straightforward way the influence of the presence of segmentation on reactivity. On the two surfaces the reaction mechanism is the same, with nucleation at steps (ridge vacancies can in fact be considered as nano-step edges) and a slow propagation. Nevertheless, when carrying out the reduction at the same reaction temperature, the second reaction step on the (10 × 2)-O surface turns out to be much faster than the reduction of the (2 × 2)$p2mg$-O structure. This difference can be rationalized by taking into account the segmentation: ridge vacancies, in fact, provide a larger number of step edges as nucleation centres; moreover, on a single segment two active sites are present, one at each end, which halves the time needed for the reaction to cover the whole segment length. We can therefore conclude that the presence of the segmentation accelerates the reduction reaction by multiplying the number of active sites.

3.2.3d. Surface oxide. The final step in the characterization of the reactivity of oxidized Rh(110) surfaces regards the reduction of the surface oxide, which is the subject of a recent XPS/STM study [48]. This system offers the opportunity to determine whether the mechanisms that apply to the adsorption systems also hold for the case of a fully oxidized surface. As already stated in section 2.1, the surface oxide is made by an O–Rh–O trilayer, containing 1.25 ML of Rh and 2.5 ML of oxygen. The reduction therefore involves a major rearrangement of metal atoms.

XPS measurements acquired while exposing the surface to molecular hydrogen at 320 K showed that the onset of the reaction is preceded by a long induction period (∼30 L H_2 exposure) during which the O 1s and Rh $3d_{5/2}$ spectra remain unchanged. Once the reaction starts, the oxide components are removed in a very narrow exposure window, leading to a final O 1s spectrum similar to those of adsorption phases. Complete reduction of the remaining adsorbed oxygen requires us to increase the temperature to ∼360 K.

The long induction period and the very fast conversion of the surface oxide to adsorption phases have been confirmed by STM experiments carried out at 370 K ($p_{H2} = 1 \times 10^{-8}$ mbar on the surface) (figure 11). As in the XPS experiments, the starting surface presents a coexistence of surface oxide regions with islands of adsorption phases (figure 11(a)). Only after ∼18 L of H_2 does a first new feature appear in the images: bright dashes homogeneously distributed over the oxide regions. The similarity of these bright dashes to those found during the initial stages of the O induced reconstruction of the Rh(110) surface (see section 3.1.1), associated with diffusing Rh–O units, points to a similar interpretation. The authors suggest that a possible source of mobile Rh–O units on the surface oxide regions is a destabilization of the thin oxide film by highly mobile H atoms penetrating the subsurface after dissociation on the same active sites during the induction period. After a few images (∼7 min), the bright dashes disappear and a c(2 × 4) array of depressions, attributed to O and/or Rh vacancies, appears on the oxide regions. In the immediately following image (32 s later, ∼0.3 L additional H_2 dose), a very sharp reaction front crosses the surface, clearly dividing it into a non-reduced region ahead of the front and a partially reduced region behind the front, as shown in figure 11(b). The partially reduced region consists of a complete rhodium layer and a few added rows that are covered by the remaining oxygen. This structurally different phase results from the

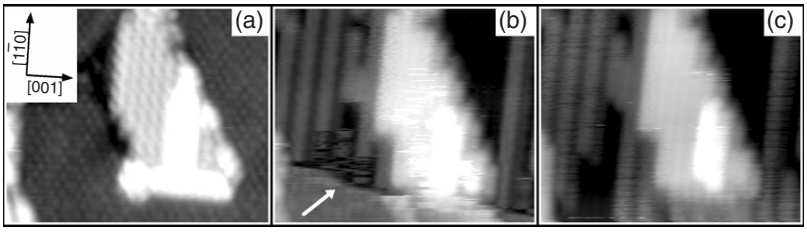

Figure 11. Hydrogen oxidation on the surface oxide. Sequence of STM images during exposure to molecular hydrogen ($p_{H2} = 1 \times 10^{-8}$ mbar, $T = 370$ K). (a) Initial surface, characterized by the coexistence of c(2×4) surface oxide areas and islands of adsorption phases, as the $(2 \times 1)p2mg$ area in the centre (42 min after starting the exposure). (b) Reaction front (indicated by the arrow), converting the surface oxide into adsorption phases. Diffusing Rh atoms are imaged immediately behind the reaction front for a few scan lines (35 s after (a)). (c) Reaction on the adsorption phases, evidenced by the presence of dark dashes on the metal rows (35 s after (b)). (Image parameters: 11×9 nm^2, $V_B = -0.6$ V, $I = 0.20$ nA, 35 s/image.)

rearrangement of the 1.25 ML rhodium atoms originally present in the surface oxide; after a few seconds (corresponding to a few scan lines) of transient mobility of Rh atoms, the added row reconstruction is stabilized by chemisorbed oxygen. Simultaneously to the surface oxide regions, the passage of the reaction front also involves the coexisting adsorption islands of the initial surface.

After the conversion of the oxide phase to adsorption phases, the reduction continues with a slower rate by following the same reaction pathway as on the $(2 \times 2)p2mg$-O surface [72] (figure 11(c)).

In conclusion, it appears that the reaction takes place mainly close to the borders between adsorption and surface oxide phase, the latter playing an active role in the overall reaction mechanism, as indicated by the formation and ordering of defects before the reaction front passage.

3.2.3e. Trends and analogies. From the detailed description of the hydrogen oxidation reaction on Rh(110) surfaces at different oxidation states we can infer some general conclusions.

On all investigated surfaces, which range from adsorption systems to surface oxide, the reaction propagates as a wavefront, which implies the presence of nucleation centres and a propagation mechanism. The rate-limiting step is the H_2 dissociation and the OH formation, which occur exclusively at defects. An atomic description of the defects which play the role of the active sites is in general not available, as, on the theory side, this would require an enormous number of DFT simulations of different configurations, while, from the experimental point of view, it is not easy to pinpoint them in the STM images. Nevertheless, in some cases it was possible to identify specific configurations that act as nucleation centres for the reaction front. This holds for example for the (10×2)-O, where STM findings were confirmed by DFT calculations, and for the $(2 \times 2)p2mg$-O, where STM measurements on large scale images allowed the onset of the reaction to be observed. In both cases it appears that the active sites are defects such as monatomic step edges of macro- or nano-lateral dimensions. The need for defects for the nucleation of the reaction indicates that a perfectly ordered, defect-free, oxygen-covered Rh(110) surface would be unreactive towards dissociative adsorption of H_2. It is interesting to note that this holds not only for saturated structures, such as the (10×2)-O (0.9 ML on the missing row reconstructed substrate), the $(2 \times 1)p2mg$-O (1 ML on the (1×1) unreconstructed substrate)

and the surface oxide, but also for lower coverage ones, such as the $(2 \times 2)p2mg$-O structure (0.5 ML on the (1×2) reconstructed substrate) and the c(2×4)-O structure (0.5 ML on the (1×1) unreconstructed substrate—the second part of the reduction of the $(2 \times 1)p2mg$-O surface).

It would be interesting to understand whether some of the features observed in detail for the case of Rh apply more generally to other TM surfaces. The similarity between the (10×2)-O structure on Rh(110) and the (12×2)-O structure on Pt(110), which therefore expose similar configurations at the atomic scale, suggests that the findings on Rh could have a more general value. Extension of this kind of studies, which couple atomic scale experimental probes with DFT calculations, to other systems, involving different metal substrates, is needed to determine the generality of this conclusion on the role of defects, which could have a key impact in understanding the behaviour of real catalysts, where defect sites are abundant.

Concerning the crucial step for the propagation of the reaction in the presented cases, it can always be traced back to the creation of free patches of rhodium atoms. Nevertheless, this result is obtained in different ways on the different surfaces, ranging from a simple rearrangement of remaining adsorbates after a partial removal to the formation of a hydrogen bond network to a combined strain removal–segmentation effect. Whenever different phases coexist on the surface, the reaction front propagates uniformly on different regions, which points to a similar efficiency of the different mechanisms that produce clean rhodium patches. This conclusion on the need for bare metal patches to dissociate H_2 might be relevant for other surfaces where it could account, for example, for distinct changes in the water production rate, as on Ru(001) [80].

Coming back to the hydrogen oxidation reaction on the Rh(110) surface, as a general rule, at $T \geqslant$ RT the reaction front is elliptical, elongated in the close-packed $[1\bar{1}0]$ direction, while it becomes more isotropic at lower temperatures. This suggests that the propagation velocities are closely related to the anisotropy of the substrate, regardless of the adsorbed layer.

Another common feature for some of the investigated surfaces is that the front removes only half of the adsorbed oxygen. This holds for the highest coverage $(2 \times 1)p2mg$-O and (10×2)-O structures. In both cases, the reaction follows a completely different pathway for the completion of the reduction. Even on the surface oxide the reaction proceeds in two stages, conversion of the oxide phase into a chemisorbed phase and complete reduction in a second stage. This common behaviour results from the interplay of different effects: the flexibility of the rhodium surface, which can easily change its structure during the reaction, the high oxygen affinity of Rh, which binds O more strongly at lower coverage, and the possible formation of hydrogen-bond networks.

4. Conclusions

The reviewed STM investigations of surface reactions on Rh(110) demonstrate the interrelation between the reactivity of this surface and the tendency of the substrate to reconstruct, when oxygen or nitrogen containing species are present as reactants or reaction products. The structural rearrangements accompanying the surface reactions are dynamical processes in continuous evolution. They depend on the adsorbate coverage and temperature, and influence the reactivity by, for example, exposing particular active sites or by affecting the diffusion. All these effects are of local nature and can hardly be accounted for by surface science techniques that yield information integrated over large areas of the surface. For this reason a local technique that is able to investigate the surface on the atomic scale, such as scanning tunnelling microscopy, can be particularly useful, providing unprecedented detail and revealing new reaction pathways. Moreover, the systems described in this review clearly demonstrate the capability of STM to follow reaction dynamics on specific regions of the surface.

Nevertheless, as the presented results have illustrated, the combination of local and non-local techniques and theoretical support is essential for an unambiguous determination of surface processes, combining details on the atomic scale with large-scale information on the surface chemical composition and linking the surface dynamics with the advancing chemical reaction. In clarifying reaction mechanisms, the contribution from theory, and its comparison to experimental data, often turned out to be crucial.

There are still limits, though, on the amount of information that can be inferred on surface reactions. First of all, the intermediate steps in catalytic processes occur on a timescale that is too fast to be accessible with the present typical STM acquisition times (of the order of a few seconds or more): only the final stage of the dynamic processes can be revealed. This is evident, for example, in the catalytic oxidation of hydrogen on reconstructed Rh(110) surfaces (see sections 3.2.3b and 3.2.3c), where no reaction intermediates (OH) were imaged but only the final situation after oxygen removal can be observed. In surface science this problem is usually sidestepped by decreasing the temperature, thus slowing down the process. This solution, however, has intrinsic drawbacks, because the reaction can follow different pathways at different temperatures, as shown for the carbon monoxide oxidation (section 3.2.1). Moreover, in the case of CO + O/Rh(110), even the LT reaction occurs in steps that cannot be directly followed with typical frame rates. Another limit of this LT approach is that the surface structure can be different at low and at high temperatures, despite the similar adsorbate coverage, especially in the case of activated substrate reconstruction, as for Rh(110).

Another limiting factor for understanding the mechanism of catalytic reactions is the lack of chemical resolution at the atomic scale, as was clearly seen for the water formation reaction on the $(2 \times 1)\,p2mg$-O/Rh(110) surface, presented in section 3.2.3a.

Finally, a fundamental restriction is the so-called pressure gap. Real catalytic processes occur at high pressure, where the actual phase of the surface can be dramatically different, due to the thermodynamic contribution of the gas phase to the surface free energy of the surface layer in the energetics through the chemical potential [81]. Furthermore, at these pressures the contaminants may play a crucial role [82].

5. Outlook

At the end of this topical review, we want to address some ongoing developments of the technique, which are promising for new deep insights into surface processes.

As outlined in the conclusions (see the previous section), one of the limits of present STM investigations of dynamical processes is a too low frame rate. This problem has been tackled by a few research groups in the last years, who developed fast STMs for UHV [83–87] and for electrochemical [88–90] applications. These new instruments allowed achieving frame-rates up to 10–25 Hz. More recently, Frenken developed a new microscope capable to go at video rate and beyond (200 Hz) [91], which will open new perspectives in the study of dynamical processes. Nevertheless, all the cited fast STMs are special, home-built, instruments, which rules out a wide spreading among research groups; new commercial fast microscopes are required for an effective impact in surface science. A parallel approach, which we are pursuing in our laboratory, is the development of fast units, which can be used as a retrofit to commercial instruments.

A hint to solve the problem of the lack of chemical resolution in STM experiments on catalytic reactions might come from inelastic tunnelling spectroscopy (IETS) [92]. This technique, which was first applied by Ho [93], exploits the injection of electrons from the tunnelling tip to detect vibrational modes of molecules as in high-resolution energy loss spectroscopy (HR-EELS), enabling the combination of real space imaging and chemical analysis at the atomic scale, and has already been used to identify reaction products [94].

Vibrational excitation by STM can also be used to manipulate single molecules on the surface [92, 95]. This allows controlling chemical reactions at the single molecule level, by inducing the single basic reaction steps, which can therefore be fully characterized [96, 97].

Nevertheless, up to now IETS has only been performed at low temperature (a few kelvin) and thus with systems far away from real catalytic conditions. Recently, Sloan and Palmer have been able to dissociate a single molecule by atomic manipulation at room temperature [98], which might open new perspectives for the future.

Chemical resolution, hence, is still a weak point in the application of the STM technique for the study of surface reactions, especially concerning the characterization of ad-species in intermediate phases. Conversely, chemical contrast for the investigation of alloy surfaces is already a matter of fact. The research group of Varga, in fact, nicely demonstrated that it is possible to discriminate in STM images between different substrate atoms, due to topography effects, differences in the LDOS (local density of states) and/or tip–surface interaction [99, 100]. The knowledge of the surface composition and chemical ordering also turned out to be essential for the understanding of adsorption on alloys, which is determined by chemical affinity, the ensemble effect and/or the ligand effect. This is a very promising field for the application of STM, as multi-component model systems are more and more considered to mimic more closely the situation typical of real catalysis.

Finally, we want to say a few words with respect to the pressure gap. In this respect, STM offers the clearest promise, as one of the few surface science techniques directly applicable in non-UHV conditions. There is a growing effort towards the development of high-pressure microscopes to study catalytic reactions at pressures ranging from UHV to atmospheric pressure [101–104]. In particular, the 'Reactor-STM' by Frenken is able to simultaneously determine the surface structure by STM and the reaction kinetics by online mass spectrometry: studies on the Pt(110) and the Pd(100) surfaces showed that the CO oxidation reaction exhibits bistability and oscillations in the kinetics that can be traced back to a cyclic metal–oxide phase transition [21, 22]. Experiments like these are opening the way to model studies of catalytic reactions in more realistic conditions, even though efforts have still to be made to achieve atomic resolution under reaction conditions.

Acknowledgments

We wish to thank our colleagues of the Surface Structure and Reactivity Group and of the Sincrotrone Trieste S.C.pA. for their invaluable contribution to many of the experiments described in this review.

We thank F Esch and M Kiskinova for scientific discussions and critical reading of the manuscript.

References

[1] Ruan L, Besenbacher F, Stensgaard I and Lægsgaard E 1992 Atom-resolved studies of the reaction between H_2S and O on Ni(110) *Phys. Rev. Lett.* **69** 3523

[2] Leibsle F M, Murray P W, Francis S M, Thornton G and Bowker M 1993 One-dimensional reactivity in catalysis studied with the scanning tunneling microscope *Nature* **363** 706

[3] Crew W W and Madix R J 1994 Monitoring surface reactions with scanning tunneling microscopy: co oxidation on p(2 × 1)-O pre-covered Cu(110) at 400 K *Surf. Sci.* **319** L34

[4] Kiskinova M 1996 Surface structure and reactivity reactions on face-centered cubic (110) metal surfaces involving adatom-induced reconstructions *Chem. Rev.* **96** 1431

[5] Murray P W, Besenbacher F and Stensgaard I 1996 Reactions on single-crystal metal surfaces studied with scanning tunneling microscopy *Israel J. Chem.* **36** 25

[6] Wintterlin J 2000 Scanning tunneling microscopy studies of catalytic reactions *Adv. Catal.* **45** 131

[7] Guo X-C and Madix R J 2003 Imaging surface reactions at atomic resolution: a wealth of behavior on the nanoscale *J. Phys. Chem.* B **107** 3105

[8] Leibsle F M, Murray P W, Condon N G and Thornton G 1997 Scanning tunneling microscopy studies of reactions on metal surfaces and model oxide supports *J. Phys. D: Appl. Phys.* **30** 741
[9] Jones A H, Poulston S, Bennet R A and Bowker M 1997 Methanol oxidation to formate on Cu(110) studied by STM *Surf. Sci.* **380** 31
[10] Bennet R A, Poulston S and Bowker M 1998 Elevated temperature scanning tunneling microscopy study of formic acid adsorption and reaction on oxygen (2 × 1) covered Cu(110) *J. Chem. Phys.* **108** 6916
[11] Bowker M, Bennet R A, Poulston S and Stone P 1998 Insights into surface reactivity: formic acid oxidation on Cu(110) studied using STM and a molecular beam reactor *Catal. Lett.* **56** 77
[12] Diebold U 2003 The surface science of titanium dioxide *Surf. Sci. Rep.* **48** 53
[13] Lai X and Goodman D W 2000 Structure–reactivity correlations for oxide-supported metal catalysts: new perspectives from STM *J. Mol. Catal.* A **162** 33
[14] Lauritsen J V, Nyberg M, Nørskov J K, Clausen B S, Topsøe H, Lægsgaard E and Besenbacher F 2004 Hydrosulfurization reaction pathways on MoS_2 nanoclusters revealed by scanning tunneling microscopy *J. Catal.* **224** 94
[15] Schoiswohl J, Eck S, Ramsey M G, Andersen J N, Surnev S and Netzer F P 2005 Vanadium oxide nanostructures on Rh(110): promotion effect of CO adsorption and oxidation *Surf. Sci.* **580** 122
[16] Sachs C, Hildebrand M, Völkening S, Wintterlin J and Ertl G 2001 Spatiotemporal self-organization in a surface reaction: from the atomic to the mesoscopic scale *Science* **293** 1635
[17] Marsh A L and Somorjai G A 2005 Structure, reactivity and mobility of carbonaceous overlayers during olefin hydrogenation on platinum and rhodium single crystal surfaces *Top. Catal.* **34** 121
[18] Tang D C, Hwang K S, Salmeron M and Somorjai G A 2004 High pressure scanning tunneling microscopy study of CO poisoning of ethylene hydrogenation on Pt(111) and Rh(111) single crystals *J. Phys. Chem.* B **108** 13300
[19] Vestergaard E K, Vang R T, Knudsen J, Pedersen T M, An T, Lægsgaard E, Stensgaard I, Hammer B and Besenbacher F 2005 Adsorbate-induced alloy phase separation: a direct view by high-pressure scanning tunneling microscopy *Phys. Rev. Lett.* **95** 126101
[20] Thorstrup P, Vestergaard E K, An T, Lægsgaard E and Besenbacher F 2003 CO-induced restructuring of Pt(110)-(1 × 2): bridging the pressure gap with high-pressure scanning tunneling microscopy *J. Chem. Phys.* **118** 3724
[21] Hendriksen B L M, Bobaru S C and Frenken J W M 2005 Looking at heterogeneous catalysis at atmospheric pressure using tunnel vision *Top. Catal.* **36** 43
[22] Hendriksen B L M, Bobaru S C and Frenken J W M 2005 Bistability and oscillations in CO oxidation studied with scanning tunneling microscopy inside a reactor *Catal. Today* **105** 234
[23] Itaya K 1998 In situ scanning tunneling microscopy in electrolyte solutions *Prog. Surf. Sci.* **58** 121
[24] Zang Z-H, Wu Z-L and Yau S-L 1999 In situ scanning tunneling microscopy imaging of well-defined Rh(111) electrodes in KNO_2-containing 0.5 M hydrofluoric acid solutions *Langmuir* **15** 8750
[25] Markovic N M and Ross P N 2002 Surface science studies of model fuel cell electrocatalysts *Surf. Sci. Rep.* **45** 121
[26] Friedrich K A, Geyzers K P, Dickinson A J and Stimming U 2002 Fundamental aspects in electrocatalysis: from the reactivity of single-crystals to fuel cell electrocatalysts *J. Electroanal. Chem.* **524/525** 261
[27] Tsiplakides D, Balomenou S, Katsaounis A, Archonta D, Koutsodontis C and Vayenas C G 2005 Electrochemical promotion of catalysis: mechanistic investigations and monolithic electropromoted reactors *Catal. Today* **100** 133
[28] Kong D S, Wan L J and Chen S H 2004 Application and research progress of electrochemical STM in corrosion science *Prog. Chem.* **16** 204
[29] Taylor K C 1984 Automobile catalytic converters *Catalysis-Science and Technology* ed J R Anderson and M Boudart (Berlin: Springer) pp 119–70
[30] Johnson–Matthey 2005 *Platinum 2005 Interim Review* p 18 http://www.platinum.matthey.com/publications/1132062873.html
[31] Somorjai G A 1996 The flexible surface: new techniques for molecular level studies of time dependent changes in metal surface structure and adsorbate structure during catalytic reactions *J. Mol. Catal.* A **107** 39
[32] Comelli G, Dhanak V R, Kiskinova M, Prince K C and Rosei R 1998 Oxygen and nitrogen interaction with rhodium single crystal surfaces *Surf. Sci. Rep.* **32** 165
[33] Baraldi A, Comelli G, Lizzit S, Kiskinova M and Paolucci G 2003 Real-time x-ray photoelectron spectroscopy of surface reactions *Surf. Sci. Rep.* **49** 169
[34] Over H, Kim Y D, Seitsonen A P, Lundgren E, Schmid M, Varga P, Morgante A and Ertl G 2000 Atomic-scale structure and catalytic reactivity of the RuO_2(110) surface *Science* **287** 1474

[35] Over H and Muhler M 2003 Catalytic CO oxidation over ruthenium-bridging the pressure gap *Prog. Surf. Sci.* **72** 3

[36] Kim S H and Wintterlin J 2004 Atomic scale investigation of the oxidation of CO on $RuO_2(110)$ by scanning tunneling microscopy *J. Phys. Chem.* B **108** 14565

[37] Reuter K, Frenkel D and Scheffler M 2004 The steady state of heterogeneous catalysis, studied by first-principles statistical mechanics *Phys. Rev. Lett.* **93** 116105

[38] Comelli G, Dhanak V R, Kiskinova M, Pangher N, Paolucci G, Prince K C and Rosei R 1992 Adsorption of oxygen on Rh(110)—a LEED, auger-electron spectroscopy and thermal-desorption study *Surf. Sci.* **260** 7

[39] Gierer M, Over H, Ertl G, Wohlgemuth H, Schwarz E and Christmann K 1993 Low-energy electron-diffraction analysis of the Rh(110)-(2 × 1)-O phase *Surf. Sci. Lett.* **297** L73

[40] Batteas J D, Barbieri A, Starkey E K, Van Hove M A and Somorjai G A 1995 The Rh(110)-p2mg(2 × 1)-2O surface-structure determined by automated tensor LEED—structure changes with oxygen coverage *Surf. Sci.* **339** 142

[41] Comelli G, Dhanak V R, Kiskinova M, Prince K C and Rosei R 1992 Adsorption of oxygen on Rh(110) and reactivity of different overlayer structures *Surf. Sci.* **269/270** 360

[42] Comicioli C, Dhanak V R, Comelli G, Astaldi C, Prince K C, Rosei R, Atrei A and Zanazzi E 1993 Structure of Rh(110)(1 × 2) and Rh(110) (2 × 2)$p2mg$-O surfaces *Chem. Phys. Lett.* **214** 438

[43] Dhanak V R, Prince K C, Rosei R, Murray P W, Leibsle F M, Bowker M and Thornton G 1994 STM study of oxygen on Rh(110) *Phys. Rev.* B **49** 5585

[44] Murray P W, Leibsle F M, Li Y, Guo Q, Bowker M, Thornton G, Dhanak V R, Prince K C and Rosei R 1993 Scanning-tunneling-microscopy study of the oxygen-induced reconstruction of Rh(110) *Phys. Rev.* B **47** 12976

[45] Hla S W, Lacovig P, Comelli G, Baraldi A, Kiskinova M and Rosei R 1999 Orientational anisotropy in oxygen dissociation on Rh(110) *Phys. Rev.* B **60** 7800

[46] Bondino F, Comelli G, Baraldi A and Rosei R 2002 Photoelectron diffraction study of the low-temperature low-coverage oxygen layer on Rh(110) *Phys. Rev.* B **66** 075402

[47] Vesselli E, Africh C, Baraldi A, Comelli G, Esch F and Rosei R 2001 (10 × 2) Strained reconstruction induced by oxygen adsorption on the Rh(110) surface *J. Chem. Phys.* **114** 4221

[48] Dudin P, Barinov A, Gregoratti L, Kiskinova M, Esch F, Dri C, Africh C and Comelli G 2005 Initial oxidation of a Rh(110) surface using atomic or molecular oxygen and titration of the surface oxide by hydrogen *J. Phys. Chem.* B **109** 13649

[49] Comelli G, Lizzit S, Hofmann Ph, Paolucci G, Kiskinova M and Rosei R 1992 Nitrogen Layers on Rh(110)1 × 1 and Rh(110)1 × 2 surfaces produced by NO + H_2 reaction—structure, stability and desorption-kinetics *Surf. Sci.* **277** 31

[50] Lizzit S, Comelli G, Hofmann Ph, Paolucci G, Kiskinova M and Rosei R 1992 Interaction of atomic nitrogen with Rh(110) *Surf. Sci.* **276** 144

[51] Kiskinova M, Lizzit S, Comelli G, Paolucci G and Rosei R 1993 Effect of the reaction conditions on the stability and structure of nitrogen layers on Rh(110) surfaces *Appl. Surf. Sci.* **64** 185

[52] Murray P W, Leibsle F M, Thornton G, Bowker M, Dhanak V R, Baraldi A, Kiskinova M and Rosei R 1994 Nitrogen-induced reconstruction on Rh(110)—effect of oxygen on the growth and ordering of Rh–N chains *Surf. Sci.* **304** 48

[53] Dhanak V R, Baraldi A, Comelli G, Prince K C, Rosei R, Atrei A and Zanazzi E 1995 Nitrogen adsorption on Rh(110) *Phys. Rev.* B **51** 1965

[54] Gierer M, Martens F, Over H, Ertl G and Imbhil R 1995 Structural-analyses of the c(2 × 4)-N + 2O and the (2 × 1)-N phases on Rh(110) by low-energy-electron diffraction *Surf. Sci.* **339** L903

[55] Besenbacher F and Nørskov J K 1993 Oxygen chemisorption on metal surfaces: general trends for Cu, Ni and Ag *Prog. Surf. Sci.* **44** 5

[56] Bennett R A, Poulston S, Jones I Z and Bowker M 1998 High-temperature scanning tunneling microscopy studies of oxygen-induced reconstructions of Pd(110) *Surf. Sci.* **401** 72

[57] Brena B, Comelli G, Ursella L and Paolucci G 1997 Oxygen on Pd(110): substrate reconstruction and adsorbate geometry by tensor LEED *Surf. Sci.* **375** 150

[58] Li W X, Österlund L, Vestergaard E K, Vang R T, Matthiesen J, Pedersen T M, Lægsgaard E, Hammer B and Besenbacher F 2004 Oxidation of Pt(110) *Phys. Rev. Lett.* **93** 146104

[59] Africh C, Esch F, Comelli G and Rosei R 2001 Dynamics of the o induced reconstruction of the Rh(110) surface: a scanning tunneling microscopy study *J. Chem. Phys.* **115** 477

[60] Comelli G, Baraldi A, Lizzit S, Cocco D, Paolucci G, Rosei R and Kiskinova M 1996 Real-time x-ray photoelectron spectroscopy study of dissociative oxygen adsorption on Rh(110) *Chem. Phys. Lett.* **261** 253

[61] Eierdal L, Besenbacher F, Lægsgaard E and Stensgaard I 1994 Interaction of oxygen with Ni(110) studied by scanning tunneling microscopy *Surf. Sci.* **312** 31
[62] Zambelli T, Barth J V and Wintterlin J 1998 Formation mechanism of the O-induced added-row reconstruction on Ag(110): a low-temperature STM study *Phys. Rev.* B **58** 12663
[63] Murray P W, Thornton G, Bowker M, Dhanak V R, Baraldi A, Rosei R and Kiskinova M 1993 Mixed O + N layers on a Rh(110) surface: competition between nitrogen and oxygen reconstructive interactions *Phys. Rev. Lett.* **71** 4369
[64] Dhanak V R, Baraldi A, Rosei R, Kiskinova M, Murray P W, Thornton G and Bowker M 1994 Reconstructive interactions in mixed N + O layers on Rh(110) *Phys. Rev.* B **50** 8807
[65] Kiskinova M 1992 Poisoning and promotion in catalysis based on surface science concepts and experiments *Studies in Surface Science and Catalysis* vol 70 (Amsterdam: Elsevier)
[66] Ertl G 2000 Dynamics of reactions at surfaces *Adv. Catal.* **45** 1
[67] Baraldi A, Lizzit S, Cocco D, Comelli G, Paolucci G, Rosei R and Kiskinova M 1997 Oxygen and carbon monoxide interactions on Rh(110) studied by real-time x-ray photoemission spectroscopy *Surf. Sci.* **385** 376
[68] Castellarin-Cudia C, Hla S W, Comelli G, Šljivananin Ž, Hammer B, Baraldi A, Prince K C and Rosei R 2001 Distinct reaction mechanisms in the catalytic oxidation of carbon monoxide on rh(110): scanning tunneling microscopy and density functional theory studies *Phys. Rev. Lett.* **87** 196104
[69] Kiskinova M, Baraldi A, Rosei R, Dhanak V R, Thornton G, Leibsle F and Bowker M 1995 Surface structural transformation during ammonia oxidation on Rh(110) *Phys. Rev.* B **52** 1532
[70] Günther S, Hoyer R, Marbach H, Imbihl R, Esch F, Africh C, Comelli G and Kiskinova M 2006 K and mixed K + O-adlayers on Rh(110) *J. Chem. Phys.* **124** 014706
[71] Africh C, Lin H, Corso M, Esch F, Rosei R, Hofer A H and Comelli G 2005 Water production reaction on Rh(110) *J. Am. Chem. Soc.* **127** 11454
[72] Africh C, Esch F, Comelli G and Rosei R 2002 Reactivity and deconstruction of the (1 × 2)-Rh(110) surface studied by scanning tunneling microscopy *J. Chem. Phys.* **116** 7200
[73] Africh C, Esch F, Li W X, Corso M, Hammer B, Rosei R and Comelli G 2004 Two-step reaction on a strained, nanoscale segmented surface *Phys. Rev. Lett.* **93** 126104
[74] Feibelman P J 2002 Partial dissociation of water on Ru(0001) *Science* **295** 99
[75] Michaelides A and Hu P 2001 Catalytic water formation on platinum: a first-principles study *J. Am. Chem. Soc.* **123** 4235
[76] Makeev A and Imbihl R 2000 Simulations of anisotropic front propagation in the $H_2 + O_2$ reaction on a Rh(110) surface *J. Chem. Phys.* **113** 3854
[77] Mertens F and Imbihl R 1995 Parameter-dependent anisotropy of front propagation in the $H_2 + O_2$ reaction on Rh(110) *Chem. Phys. Lett.* **242** 221
[78] Cvetko D, Floreano L, Morgante A, Peloi M, Tommasini F, Prince K C, Vendruscolo M and Tosatti E 1994 Evolution of the missing row deconstruction on Rh(110) *Surf. Sci.* **318** L1193
[79] Baraldi A, Lizzit S, Bondino F, Comelli G, Rosei R, Sbraccia C, Bonini N, Baroni S, Mikkelsen A and Andersen J N 2005 Thermal stability of the Rh(110) missing-row reconstruction: combination of real-time core-level spectroscopy and ab-initio modeling *Phys. Rev.* B **72** 075417
[80] Koch M H, Jakob P and Menzel D 1996 The influence of steps on the water-formation reaction on Ru(001) *Surf. Sci.* **367** 293
[81] Reuter K and Scheffler M 2001 Composition, structure, and stability of RuO_2(110) as a function of oxygen pressure *Phys. Rev.* B **65** 035406
[82] Starr D E, Shaikhutdinov S K and Freund H J 2005 Gold supported on oxide surfaces: environmental effects as studied by STM *Top. Catal.* **36** 33
[83] Kuipers L, Loos R W M, Neerings H, ter Horst J, Ruwiel G J, de Jongh A P and Frenken J W M 1995 Design and performance of a high-temperature, high-speed scanning tunneling microscope *Rev. Sci. Instrum.* **66** 4557
[84] Hoogeman M S, Schößer D C, Sanders J B, Kuipers L and Frenken J W M 1996 Surface energetics and thermal roughening of Ag(115) studied with STM movies *Phys. Rev.* B **53** R13299
[85] Wintterlin J, Trost J, Renisch S, Schuster R, Zambelli T and Ertl G 1997 Real-time STM observations of atomic equilibrium fluctuations in an adsorbate system: O/Ru(0001) *Surf. Sci.* **394** 159
[86] Mendez J, Kim S H, Cerdá J, Wintterlin J and Ertl G 2005 Coadsorption phases of co and oxygen on Pd(111) studied by scanning tunneling microscopy *Phys. Rev.* B **71** 085409
[87] Curtis R, Mitsui T and Ganz E 1997 An ultrahigh vacuum high speed scanning tunneling microscope *Rev. Sci. Instrum.* **68** 2790
[88] Magnussen O M, Zitzler L, Gleich B, Vogt M R and Behm R J 2001 In-situ atomic-scale studies of the mechanisms and dynamics of metal dissolution by high-speed STM *Electrochim. Acta* **46** 3725

[89] Polewska W, Behm R J and Magnussen O M 2003 In-situ video-stm studies of Cu electrodeposition on Cu(100) in HCl solution *Electrochim. Acta* **48** 2915
[90] Labayen M and Magnussen O M 2004 In situ video-STM study of the potential-induced (1 × 1) → 'hex' transition on Au(100) electrode surfaces in Cl^- containing solution *Surf. Sci.* **573** 128
[91] Rost M J, Crama L, Schakel P, van Tol E, van Velzen-Williams G B E M, Overgauw C F, ter Horst, Dekker H, Okhuijsen B, Seynen M, Vijftigschild A, Han P, Katan A J, Schoots K, Schumm R, van Loo W, Oosterkamp T H and Frenken J W M 2005 Scanning probe microscopes go video rate and beyond *Rev. Sci. Instrum.* **76** 053710
[92] Komeda T 2005 Chemical identification and manipulation of molecules by vibrational excitation via inelastic tunneling process with scanning tunneling microscopy *Prog. Surf. Sci.* **78** 41
[93] Stipe B C, Razaei M A and Ho W 1998 Single-molecule vibrational spectroscopy and microscopy *Science* **280** 1732
[94] Lauhon L J and Ho W 2000 The initiation and characterization of single bimolecular reactions with a scanning tunneling microscope *Faraday Discuss.* **117** 249
[95] Ueba H 2003 Motions and reactions of single adsorbed molecules induced by vibrational excitation with STM *Surf. Rev. Lett.* **10** 771
[96] Hla S W and Rieder K H 2003 STM control of chemical reactions: single-molecule synthesis *Annu. Rev. Phys. Chem.* **54** 307
[97] Hla S W, Meyer G and Rieder K H 2001 Inducing single-molecule chemical reactions with a UHV-STM: a new dimension for nano-science and technology *ChemPhysChem* **2** 361
[98] Sloan P A and Palmer R E 2005 Two-electron dissociation of single molecules by atomic manipulation at room temperature *Nature* **434** 367
[99] Varga P and Schmid M 1999 Chemical discrimination on atomic level by STM *Appl. Surf. Sci.* **141** 287
[100] Schmid M and Varga P 2002 Segregation and surface chemical ordering—an experimental view on the atomic scale *The Chemical Physics of Solid Surfaces* vol 10 *Alloy Surfaces and Surface Alloys* ed D P Woodruff (Amsterdam: Elsevier)
[101] Rößler M, Geng P and Wintterlin J 2005 A high-pressure scanning tunneling microscope for studying heterogeneous catalysis *Rev. Sci. Instrum.* **76** 023705
[102] Lægsgaard E, Osterlund L, Thostrup P, Rasmussen P B, Stensgaard I and Besenbacher F 2001 A high-pressure scanning tunneling microscope *Rev. Sci. Instrum.* **72** 3537
[103] Rasmussen P B, Hendriksen B L M, Zeijlemaker H, Ficke H G and Frenken J W M 1998 The 'reactor STM': a scanning tunneling microscope for investigation of catalytic surfaces at semi-industrial reaction conditions *Rev. Sci. Instrum.* **69** 3879
[104] Jensen J A, Rider K B, Chen Y, Salmeron M and Somorjai G A 1999 High pressure, high temperature scanning tunneling microscopy *J. Vac. Sci. Technol.* B **17** 1080